CZECH TECHNICAL UNIVERSITY IN PRAGUE
Faculty of nuclear sciences and physical engineering
Department of physics

The forward - backward asymmetry of electrons coming from Z^0 boson decay in proton - proton interactions with 14 TeV center of mass energy.

research work

Supervisor RNDr. Pavel Staroba CSc.

Jan Čepila

2006

Title:
The forward - backward asymmetry of electrons coming from Z boson decay in proton - proton interactions with 14 TeV center of mass energy

Author: Jan Čepila

Specialization: Experimental nuclear physics

Sort of project: Research work

Supervisor: RNDr. Pavel Staroba, CSc. Division of Elementary Particle Physics, Institute of Physics, Academy of Sciences of the Czech Republic.

Consultant:

Abstract: The current best formulated particle theory is the Standard Model. It explains the basic phenomena of interactions between particles. Almost all particle physics experiments are dedicated to the verification or even extension of this model. The biggest of such experiments is the ATLAS experiment on the LHC accelerator in CERN in recent times. Several parts of the Standard model are studied there and they will be presented in more details in this work. Mainly, we will insist on Drell-Yan process of lepton pair production via the Z boson. Appropriate theoretic framework is also presented for better understanding of the whole process. This work is devoted to the forward-backward asymmetry of lepton pair production in particular. Using that the Weinberg angle, Higgs boson mass estimation etc. can be elaborated. However, the Standard model is probably not the ultimate theory. It has many unanswered questions and problems. That is why many alternative theories going beyond the Standard Model are being studied.

Key words: Drell-Yann process, forward-backward asymmetry, Weinberg angle, ATLAS, ROOT, Pythia, Herwig.

Název práce:
Zkoumání předo-zadní asymetrie výletu elektronů z rozpadu bosonu Z v proton-protonových srážkách při těžišt'ové energii 14TeV

Autor: Jan Čepila

Abstrakt: Standardní model je dnes nejpropracovanější teorií zabývající se částicemi a jejich vzájemnými interakcemi. Ověřením platnosti a případně jeho rozšířením se zabývají všechny současné experimenty v oblasti částicové fyziky. Největším

z experimentů je v současné době experiment ATLAS na urychlovači LHC v CERN. Zde je studováno několik oblastí standardního modelu, které jsou rozebrány podrobněji v této práci. Zvláštní důraz je kladen na Drell-Yanovský proces produkce leptonového páru prostřednictvím bosonu Z. Potřebné teoretické výpočty jsou předloženy pro snadnější pochopení celého procesu. Konkrétní vlastnost, které je věnována tato práce je předo-zadní asymetrie výletu leptonového páru. Pomocí ní lze zpřesnit například hodnotu Weinbergova úhlu, nebo odhad na hmotu Higgsova bosonu apod. I přes mnohé potvrzení Standardního modelu, i tato teorie má mnoho nezodpovězených otázek a problémů. Proto vznikají a studují se i další teorie jdoucí za hranice Standardního modelu.

Klíčová slova: Drell-Yannovský proces, předo-zadní asymetrie, Weinbergův úhel, ATLAS, ROOT, Pythia, Herwig.

Contents

1 Introduction **6**

2 Theoretical framework **7**
2.1 GWS Standard model review 7
2.2 QCD factorization theorem for Drell-Yan process 12
2.3 The parton model cross-section calculation background 15
2.4 Calculation of partonic cross-sections in hadron collisions 17
2.4.1 Leading-order calculations 17
2.4.2 Next-to-leading-order calculations 21
2.4.3 Next-to-next-to-leading-order calculations 23
2.4.4 All orders approach 23
2.4.5 Parton distribution functions 24
2.5 Drell-Yan pair production cross-section calculation 25

3 Programs for generating events - Pythia **28**

4 ATLAS physics overview **32**
4.1 QCD processes at the LHC 33
4.1.1 Drell-Yan physics 33
4.2 Physics of electroweak gauge bosons 37
4.3 B-physics 38
4.4 Heavy quarks and leptons 38
4.5 Higgs boson(s) 39
4.6 Beyond Standard model 41

5 Results of analysis **42**
5.1 Files, analysis tools 42
5.2 Event selection, analyzed objects 43
5.3 Dependence of forward-backward asymmetry and kinematics distributions on the cuts applied on the secondary electrons 43

6 Conclusions **53**

Appendices **54**

7 References **56**
7.1 Bibliography 56

List of Figures

2.1 Feynmann diagrams of all possible interactions[4] 13
2.2 Schematics of Drell-Yan factorization theorem 15
2.3 The schematics of electron-hadron scattering[3] 16
2.4 Feynman diagrams for W+1 production 17
2.5 Feynman diagrams for W+1 production as 2→2 scattering 19
2.6 Feynman diagrams for W+2 production 19
2.7 Feynman diagrams NLO approximation 22

4.1 Feynmann diagram of Drell-Yan process 33
4.2 Cross-section of Drell-Yan muon production as a function of its invariant mass[6] 35
4.3 The Z boson production cross-section as a function of its transverse momentum[6] 35
4.4 Feynman diagrams for heavy quarks production 39
4.5 Feynman diagrams for Higgs boson production 40
4.6 Feynman diagrams for Higgs boson production 41

5.1 Drell-Yan process via Z boson only 42
5.2 Drell-Yan process via Z boson and gamma 43
5.3 Asymetry bar chart 45
5.4 The rapidity distribution for generated Z boson from the first set 46
5.5 The p_T distribution for generated Z boson from the first set . . . 46
5.6 The rapidity distribution for generated Z boson from the second set 46
5.7 The p_T distribution for generated Z boson from the second set . 47
5.8 Fitting functions for invariant mass distribution 47
5.9 fitted mean for Z boson mass distributions for generated Z boson 48
5.10 fitted gamma for Z boson mass distributions for generated Z boson 48
5.11 fitted χ^2/ndf for Z boson mass distributions for generated Z boson 49
5.12 fitted mean for Z boson mass distributions for secondary Z boson 50
5.13 fitted gamma for Z mass distributions for secondary Z boson . . 50
5.14 fitted χ^2/ndf for Z mass distributions for secondary Z boson . . 51
5.15 fitted mean for Z boson p_T distributions 51
5.16 Rapidity distributions for each cut 52

Chapter 1

Introduction

This project is devoted to the study of the forward - backward asymmetry of electrons coming from the Z boson decay in proton - proton interactions with 14 TeV center of mass energy. Proper theoretical framework concerning physics on hadron colliders is presented including the computation of cross sections on hadronic accelerators. For the purpose of this analysis, the Drell-Yan process leading to the electron-positron pair was chosen. For this reason, a short remind of GWS theory is included and the cross-section is calculated for this process particularly. Because the ATLAS experiment on LHC accelerator is still not running, we have to make this analysis on the generator level. Physics background of the process of generating events is also included. Next chapter summarizes several topics of the Standard model that are studied on ATLAS detector. Also several kinematical variables of Z boson are studied, in particular, their dependence on various kinematic cuts. This work was presented on the Standard Model Working Group ATLAS phone meeting[10] in 7th June 2007 and on Physics In Collision conference 2007 in Annecy, France.

Chapter 2

Theoretical framework

2.1 GWS Standard model review

The Glashow-Weinberg-Salam theory of electroweak interactions forms a cornerstone of theory known as Standard model. Conclusions coming from this theory are well-verified (excluding Higgs field) in wide range of energies. This model incorporates

3 generations of leptons - $e^-, \nu_e, \mu^-, \nu_\mu, \tau^-, \nu_\tau$ with spin $\frac{1}{2}$
6 quarks - d, u, s, c, b, t with spin $\frac{1}{2}$
4 intermedial bosons $W^\pm, Z^0, \gamma$ with spin 1
Higgs boson H with spin 0

Fermions are believed to be constituents of matter, bosons are mediators of united electroweak interaction. The Higgs field is connected with generating of the mass of other particles.
The fundamental principle on which the theory is built is a local gauge invariance. This principle is believed to be the leading rule of all physics in this region. Such belief is due to the agreement of this type of theories with experimental data. The correspondent group of symmetries is non-abelian $SU_{(2)} \times U_{(1)}$, which is usually called weak isospin times weak hypercharge group. The mediators $W^\pm, Z^0, \gamma$ are quanta of physical vector fields, composed of original Yang-Mills fields, which are connected with generators of $SU_{(2)} \times U_{(1)}$.
The fermion sector is composed of left-handed doublets

$$L^{(e)} = \begin{pmatrix} \nu_{eL} \\ e_L \end{pmatrix} \quad L^{(\mu)} = \begin{pmatrix} \nu_{\mu L} \\ \mu_L \end{pmatrix} \quad L^{(\tau)} = \begin{pmatrix} \nu_{\tau L} \\ \tau_L \end{pmatrix}$$
$$L_0^{(d)} = \begin{pmatrix} u_{0L} \\ d_{0L} \end{pmatrix} \quad L_0^{(s)} = \begin{pmatrix} c_{0L} \\ s_{0L} \end{pmatrix} \quad L_0^{(b)} = \begin{pmatrix} b_{0L} \\ t_{0L} \end{pmatrix},$$

where q_{0L} are so called primordial fields(or protofields), because they do not represent physical entity. It is necessary to transform them to physical fields

with definite mass.

The second part is composed of right-handed singlets

$$\begin{array}{ccccccc} & & e_R & \mu_R & \tau_R & & \\ d_{0R} & u_{0R} & c_{0R} & s_{0R} & b_{0R} & t_{0R} \end{array}$$

We have used the notation $e_L = \frac{1}{2}(1-\gamma_5)e$ and $e_R = \frac{1}{2}(1+\gamma_5)e$. The local gauge invariance of $SU_{(2)} \times U_{(1)}$ gives us proper Lagrangian terms describing fermion kinematics and interaction with gauge fields. The problem is, that the potential in Lagrangian has wrong sign in mass term. This can be corrected with the spontaneous symmetry breaking. Shifting this potential to variables with the minimum at vacuum expectation value, we obtain correct fermion mass term. The third principle, we have to use is Higgs mechanism. Then, we can then generate correct masses for gauge fields and get rid of Goldstone bosons only just by picking proper gauge transformation. For that, we will use the $SU_{(2)}$ doublet of complex scalar fields

$$\Phi = \begin{pmatrix} \varphi^+ \\ \varphi^0 \end{pmatrix}$$

and a conjugate variant

$$\tilde{\Phi} = i\tau_2 \Phi^*.$$

The final Lagrangian is of the form

$$\mathcal{L}_{GWS} = \mathcal{L}_{gauge} + \mathcal{L}_{fermion} + \mathcal{L}_{Higgs} + \mathcal{L}_{Yukawa}$$

$\mathcal{L}_{\mathbf{gauge}}$: pure Yang-Mills part of Lagrangian, connected to the local symmetry $SU_{(2)} \times U_{(1)}$

$$\mathcal{L}_{gauge} = -\frac{1}{4} F^a_{\mu\nu} F^{a\mu\nu} - \frac{1}{4} B_{\mu\nu} B^{\mu\nu},$$

where $F^a_{\mu\nu} = \partial_\mu A^a_\nu - \partial_\nu A^a_\mu + g\epsilon^{abc} A^b_\mu A^c_\nu$ and $B_{\mu\nu} = \partial_\mu B_\nu - \partial_\nu B_\mu$. This term implements one constant g, called gauge coupling constant.

$\mathcal{L}_{\mathbf{fermion}}$:lepton and quark kinetic term, including their interaction with gauge fields

$$\begin{aligned}\mathcal{L}_{fermion} = &\sum_{l=e,\mu,\tau} i\bar{L}^{(l)}\gamma^\mu(\partial_\mu - igA^a_\mu\frac{\tau^a}{2} - iY_L^{(l)}g`B_\mu)L^{(l)} \\ &+ \sum_{q=d,s,b} i\bar{L}_0^{(q)}\gamma^\mu(\partial_\mu - igA^a_\mu\frac{\tau^a}{2} - iY_L^{(q)}g`B_\mu)L_0^{(q)} \\ &+ \sum_{l=e,\mu,\tau} i\bar{l}_R\gamma^\mu(\partial_\mu - iY_R^{(q)}g`B_\mu)l_R \\ &+ \sum_{q=d,u,s,c,b,t} i\bar{q}_{0R}\gamma^\mu(\partial_\mu - iY_R^{(q)}g`B_\mu)q_{0R}\end{aligned}$$

If we consider known properties of described particles, we can substitute

$$\begin{aligned}Y = Q - T_3 \quad \Rightarrow \quad Y_L^{(l)} &= -\frac{1}{2}\ l = e,\mu,\tau \\ Y_L^{(q)} &= \frac{1}{6}\ q = d,s,b \\ Y_R^{(q)} &= -\frac{1}{3}\ q = d,s,b \\ Y_R^{(q)} &= \frac{2}{3}\ q = u,c,t\end{aligned}$$

Another constant is given here, namely $g`$ - the electromagnetic coupling constant.

$\mathcal{L}_{\mathbf{Higgs}}$:mass and interactions of the Higgs field

$$\mathcal{L}_{Higgs} = \Phi^\dagger(\partial_\mu + igA^a_\mu\frac{\tau^a}{2} + \frac{i}{2}g`B_\mu)(\partial^\mu - igA^{b\mu}\frac{\tau^b}{2} - \frac{i}{2}g`B_\mu)\Phi - \lambda(\Phi^\dagger\Phi - \frac{v^2}{2})^2,$$

where λ is the self-interaction coupling constant and v is vacuum expectation value.

$\mathcal{L}_{\mathbf{Yukawa}}$:

$$\begin{aligned}\mathcal{L}_{Yukawa} = &-\sum_{l=e,\mu,\tau}(h_l\bar{L}^{(l)}\Phi l_R + (h_l\bar{L}^{(l)}\Phi l_R)^\dagger) \\ &-\sum_{q=d,s,b;q`=d,s,b}(h_{qq`}\bar{L}_0^{(q)}\Phi q`_{0R} + (h_{qq`}\bar{L}_0^{(q)}\Phi q`_{0R})^\dagger) \\ &-\sum_{q=d,s,b;q`=u,c,t}(\tilde{h}_{qq`}\bar{L}_0^{(q)}\tilde{\Phi} q`_{0R} + (\tilde{h}_{qq`}\bar{L}_0^{(q)}\tilde{\Phi} q`_{0R})^\dagger)\end{aligned}$$

Again, $h_l, h_{qq`}, \tilde{h}_{qq`}$ are coupling constants(arbitrary).

The complex doublet $\Phi = \begin{pmatrix} \varphi^+ \\ \varphi^0 \end{pmatrix}$ contains 4 real scalars - 3 of them corresponds to Goldstone bosons of spontaneously broken $SU_{(2)}$ symmetry from the Higgs potential. These scalar fields can be avoided with a proper selection of gauge transformation

$$\Phi_U = \begin{pmatrix} 0 \\ \frac{1}{\sqrt{2}}(v+H) \end{pmatrix}$$
$$\tilde{\Phi}_U = \begin{pmatrix} \frac{1}{\sqrt{2}}(v+H) \\ 0 \end{pmatrix}$$

Fields in final Lagrangian are not "physical" because they do not describe any particle. This can be done by their linear combination

$W_\mu^\pm = \frac{1}{\sqrt{2}}(A_\mu^1 \mp iA_\mu^2)$ ... weak charged current

$A_\mu^3 = cos\Theta_W Z_\mu + sin\Theta_W A_\mu$ ... weak neutral current

$B_\mu = -sin\Theta_W Z_\mu + cos\Theta_W A_\mu$ (decays into Z^0 and γ)

So, we can transform from non-physical fields $A_\mu^1, A_\mu^2, A_\mu^3, B_\mu$ to measurable fields $W_\mu^\pm, Z_\mu, A_\mu$. We can see, that neutral currents are only a linear combination of the neutral weak mediator Z^0 and the neutral electromagnetic mediator γ. Coefficients of this combination are due to the so called Weinberg angle Θ_W. From

$$cos\Theta_W = \frac{g}{\sqrt{g^2 + g^{`2}}} \qquad e = \frac{gg^`}{\sqrt{g^2 + g^{`2}}}$$

therefore

$$e = g^`cos\Theta_W$$
$$e = gsin\Theta_W$$

If we move from protofields[4] to physical fields, we can rewrite the kinetic part of $\mathcal{L}_{gauge}$ as

$$\mathcal{L}_{gauge}^{kin.part} = -\frac{1}{2}W_{\mu\nu}^- W_{\mu\nu}^+ - \frac{1}{4}Z_{\mu\nu}Z^{\mu\nu} - \frac{1}{4}A_{\mu\nu}A^{\mu\nu},$$

where $W_{\mu\nu}^- = \partial_\mu W_\nu^- - \partial_\nu W_\mu^-$. These terms represent a self-interaction of vector bosons of types $WW\gamma$, WWZ, $WWWW$, $WWZZ$, $WWZ\gamma$ and $WW\gamma\gamma$. Other types are not included in this part of Lagrangian(between bosons).
From the Higgs sector it is obvious that $m_H^2 = 2\lambda v^2$. Other masses are generated by the Higgs mechanism which gives results such that

$$\left.\begin{array}{c} m_W = \frac{1}{2}gv \\ m_Z = \frac{1}{2}\sqrt{g^2 + g^{\prime 2}}v \end{array}\right\} \quad m_W = m_Z cos\Theta_W$$

For the vacuum ground state it can be derived (using Fermi constant)

$$v = \frac{1}{\sqrt{G_F\sqrt{2}}} \doteq 246GeV$$

Furthermore, the Higgs sector contains following self-interactions and interactions with bosonic fields - WWH, ZZH, $WWHH$, $ZZHH$, HHH, $HHHH$.

The mass of charged leptons comes from Yukawa's part of the Lagrangian

$$m_l = \frac{1}{\sqrt{2}}h_l v,$$

so there rise a pure scalar Yukawa interaction of the type llH. In quark sector, it is much more difficult. There are 2 matrices 3×3 for primordial fields. It leads to the qqH type interaction. Both matrices can be diagonalized with a proper biunitary transformation[4]. Using this, we can rewrite quark part of the Lagrangian $\mathcal{L}_{fermion}$ in order to obtain physical fields with a well defined mass

$$\begin{pmatrix} d_L \\ s_L \\ b_L \end{pmatrix} = U \begin{pmatrix} d_{0L} \\ s_{0L} \\ b_{0L} \end{pmatrix} \quad \begin{pmatrix} u_L \\ c_L \\ t_L \end{pmatrix} = \tilde{U} \begin{pmatrix} u_{0L} \\ c_{0L} \\ t_{0L} \end{pmatrix} ,$$

where U and $\tilde{U}$ are unitary matrices 3×3 different in general. More interesting than these two matrices is a matrix

$$V = \tilde{U}U^{\dagger} = \begin{pmatrix} V_{ud} & V_{us} & V_{ub} \\ V_{cd} & V_{cs} & V_{cb} \\ V_{td} & V_{ts} & V_{tb} \end{pmatrix}$$

This is the well-known Cabbibo-Kobayashi-Maskawa matrix. It can be parametrized by 4 Cabbibo angles and 1 CP violating phase. If we want to incorporate massive neutrinos and their mixing into the Standard model, we can proceed in similar way. By adding right-handed singlets for neutrinos, we can use a technique for derivation of quark masses as well for leptons in Yukawa's part of Lagrangian. Now we can get Dirac mass terms for neutrinos as well as Yukawa's interaction with the Higgs particle and lepton analogy of CKM matrix.

Finally, we will rewrite the interaction part of Lagrangian in U-gauge.

$$\begin{aligned}
\mathcal{L}_{int}^{GWS} = & \sum_f Q_f e \bar{f} \gamma^\mu f A_\mu + \mathcal{L}_{CC} + \mathcal{L}_{NC} \\
& -ig(W_\mu^0 W_\nu^- \overleftrightarrow{\partial^\mu} W^{+\nu} + W_\mu^- W_\nu^+ \overleftrightarrow{\partial^\mu} W^{0\nu} + W_\mu^+ W_\nu^0 \overleftrightarrow{\partial^\mu} W^{-\nu}) \\
& -g^2(\tfrac{1}{2}(W^-W^+)^2 - \tfrac{1}{2}(W^-)^2(W^+)^2 + (W^0)^2(W^-W^+) - (W^-W^0)(W^+W^0)) \\
& +gm_W W_\mu^- W^{+\mu} H + \tfrac{1}{2cos\Theta_W} g m_Z Z_\mu Z^\mu H \\
& +\tfrac{1}{4} g^2 W_\mu^- W^{+\mu} H^2 + \tfrac{1}{8} \tfrac{g^2}{cos^2\Theta_W} Z_\mu Z^\mu H^2 \\
& -\sum_f \tfrac{1}{2} g \tfrac{m_f}{m_W} \bar{f} f H - \tfrac{1}{4} g \tfrac{m_H^2}{m_W} H^3 - \tfrac{1}{32} g^2 \tfrac{m_H^2}{m_W^2} H^4
\end{aligned}$$

The summation index goes through all fermions and the symbol W_μ^0 stands for the field A_μ^3.

$$\mathcal{L}_{CC} = \frac{g}{2\sqrt{2}} \sum_{l=e,\mu,\tau} \bar{\nu}_e \gamma^\lambda (1-\gamma_5) e W_\lambda^+ + \frac{g}{2\sqrt{2}} (\bar{u}, \bar{c}, \bar{t}) \gamma^\lambda (1-\gamma_5) V_{CKM} \begin{pmatrix} d \\ s \\ b \end{pmatrix} W_\lambda^+ + hermit.conj.part$$

$$\mathcal{L}_{NC} = \frac{g}{cos\Theta_W} \sum_f (\epsilon_L^{(f)} \bar{f}_L \gamma^\lambda f_L + \epsilon_R^{(f)} \bar{f}_R \gamma^\lambda f_R) Z_\lambda$$

$$\begin{aligned}
\epsilon_L^{(f)} &= T_{3L}^{(f)} - Q_f sin^2\Theta_W \\
\epsilon_R^{(f)} &= T_{3R}^{(f)} - Q_f sin^2\Theta_W
\end{aligned}$$

Parameters of Standard model can be expressed equivalently as

$$g, g`, \lambda, v \Leftrightarrow \alpha, sin^2\Theta_W, m_Z, m_H \Leftrightarrow \alpha, G_F, m_Z, m_H$$

These are main parameters coming from a gauge principle, other parameters comes from the Yukawa sector. Namely 3 masses of charged leptons(without neutrinos), 6 masses of quarks and 4 cabbibo parameters. This means 17 parameters for the whole GWS model(24 with neutrinos being massive).

2.2 QCD factorization theorem for Drell-Yan process

At high energy hadron colliders, we can distinguish two types of scattering processes. Higgs boson and high p_T jet production are denoted as hard processes

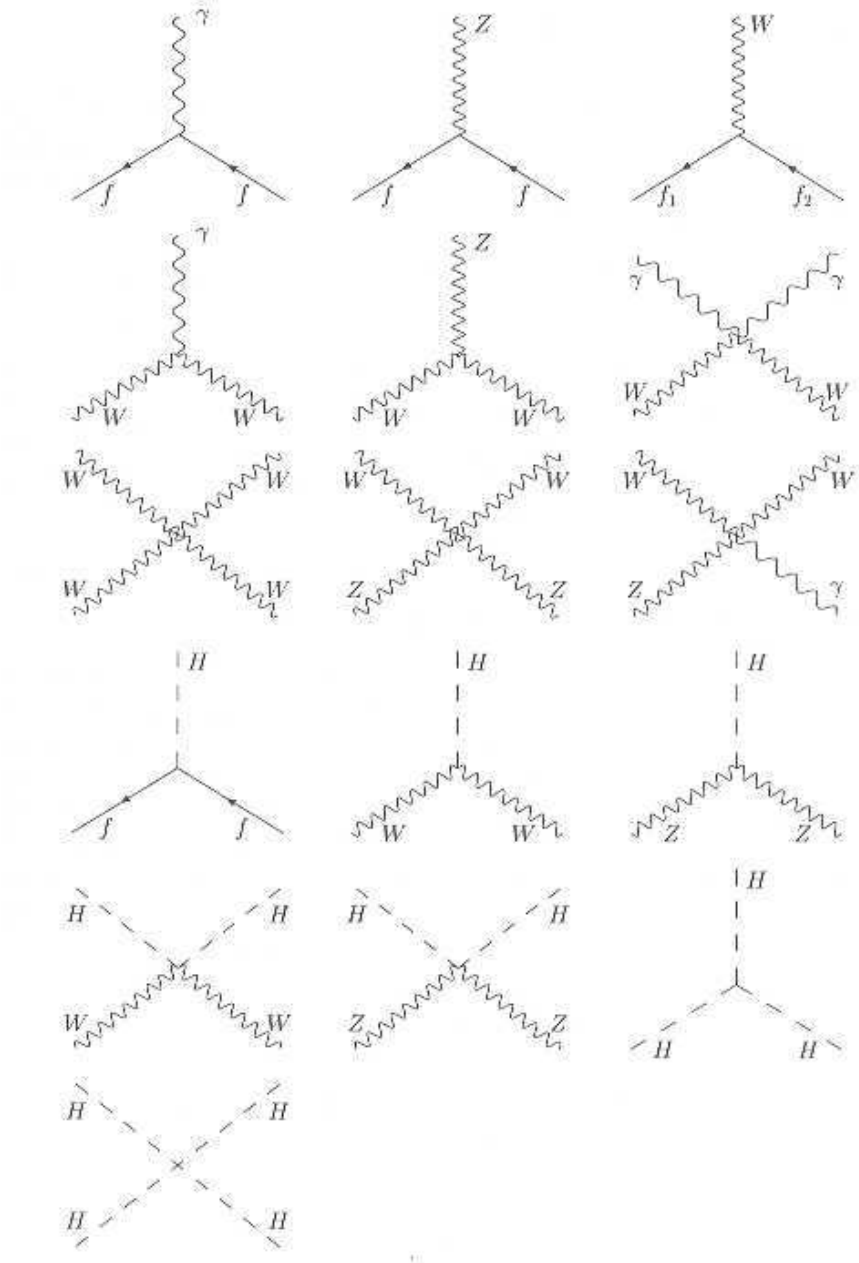

Figure 2.1: Feynmann diagrams of all possible interactions[4]

and their rates and properties can be predicted very well with perturbation theory. The total cross-section and underlying events are called soft processes, which are lead by non-perturbative QCD effects. All those processes are still described by the QCD theory. Furthermore, hard processes are followed by soft interactions and therefore they have to be well analyzed to obtain comparable predictions from perturbative approach. The factorization in QCD can be used to obtain such hard scattering cross-sections in hadron-hadron collisions. Here we will restrict to leading order processes (LO). The factorization theorem comes from Drell and Yan. They suggested that the parton model ideas which comes from the deep inelastic scattering can be used on certain processes in hadron-hadron collisions. They studied the production of massive lepton pair by quark-antiquark annihilation (see Drell-Yan process section). They postulated that the hadronic cross-section of the process $AB \to e^+e^- + X$ is[2]

$$\sigma_{AB} = \int \mathrm{dx_a dx_b f_{a/A}(x_a) f_{b/B}(x_b) \hat{\sigma}_{q\bar{q}\to e^+e^-}}$$

where $f_{g/A}(x)$ are parton distribution functions from the deep inelastic scattering. The domain of validity is the asymptotic limit (in analogy of Bjorken scaling limit) $\tau = \frac{M^2_{l^+l^-}}{s}|_{s\to+\infty}$ fixed. The same approach can be used to other hard scattering processes. Problems arise when we calculate perturbative corrections from real and virtual gluon emission. Large logarithms from gluons emitted collinear with incoming quarks appeared to spoil the convergence of the perturbative expansion. This is the same problem as in deep inelastic scattering structure function calculations. So they can be absorbed (using DGLAP equations in the definition of the parton distributions) giving rise to logarithmic violations of scaling. All logarithms from Drell-Yan corrections can be factored into renormalized parton distributions as they appear in the factorization theorem. Restricting to LO logarithm corrections we can write[2]

$$\sigma_{AB} = \int \mathrm{dx_a dx_b f_{a/A}(x_a, Q^2) f_{b/B}(x_b, Q^2) \hat{\sigma}_{q\bar{q}\to e^+e^-}}$$

The factor Q^2 is a large momentum scale, which characterizes the hard scattering. Changes to the Q^2 scale of $O(1)$ are equivalent in this leading logarithm approximation. The last step is the fact that the finite corrections after factorization of logarithms had to be calculated separately for each process (perturbative $O(\alpha_S^n)$ correction to the total cross-section). Therefore

$$\sigma_{AB} = \int \mathrm{dx_a dx_b f_{a/A}(x_a, \mu_F^2) f_{b/B}(x_b, \mu_F^2)} \times [\hat{\sigma}_0 + \alpha_S(\mu_R^2)\hat{\sigma}_1 + \ldots]_{q\bar{q}\to e^+e^-}$$

where μ_F is a factorization scale, which "separates" the long and short-distance physics. The μ_R is a renormalization scale for the QCD running coupling. Formally, the total cross-section (to all orders of PT) is invariant under changes in these parameters. In the absence of a complete set of higher order corrections, it is necessary to make a choice for these scales to make cross-section

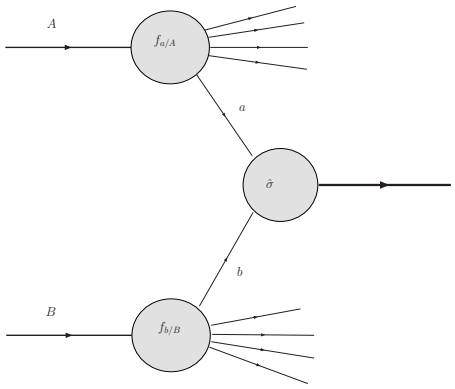

Figure 2.2: Schematics of Drell-Yan factorization theorem

predictions. For Drell-Yan process, the standard choice is $\mu_F = \mu_R = M_{l^+l^-}$. The DGLAP equations are[2]

$$\frac{\partial q_i(x,\mu^2)}{\partial log\mu^2} = \frac{\alpha_S}{2\pi}\int_x^1 \frac{dz}{z}[P_{q_iq_j}(z,\alpha_S)q_j(\frac{x}{z},\mu^2) + P_{q_ig}(z,\alpha_S)g(\frac{x}{z},\mu^2)]$$
$$\frac{\partial g(x,\mu^2)}{\partial log\mu^2} = \frac{\alpha_S}{2\pi}\int_x^1 \frac{dz}{z}[P_{gq_j}(z,\alpha_S)q_j(\frac{x}{z},\mu^2) + P_{gg}(z,\alpha_S)g(\frac{x}{z},\mu^2)]$$

where P_{ab} are splitting functions with perturbative expansion

$$P_{ab}(x,\alpha_S) = P_{ab}^{(0)}(x) + \frac{\alpha_S}{2\pi}P_{ab}^{(1)}(x) + \dots$$

.

These equations determine the Q^2 dependence of the pdfs. The x-dependence has to be obtained from fitting hard scattering data.

2.3 The parton model cross-section calculation background

The parton model was developed to describe the observation of scaling in hadronic processes. It is interpreted as a consequence of charged point-like constituents in hadron, called quarks of QCD. It is assumed that any physically observed hadron consists of partons(identified with quarks and gluons). Because of the scale of the hadron scattering and because of the high energy of colliding particles, the masses of hadrons and partons can be neglected[3]. Therefore it can be seen that the hadron four-momentum p^μ meets the relation

$$p^2 = \frac{E^2}{c^2} - \vec{p}^2 = \frac{m^2c^4 + \vec{p}^2c^2}{c^2} - \vec{p}^2 = m^2c^2 = 0$$

Furthermore, every relevant parton in the hard scattering has a momentum xp^{μ}, where $x \in < 0, 1 >$. The parton model cross-section is calculated from no-loop tree diagrams of partonic scattering using the factorization theorem (see previous section). The calculation is based on the deep inelastic scattering of lepton (point-like particle) on hadrons.

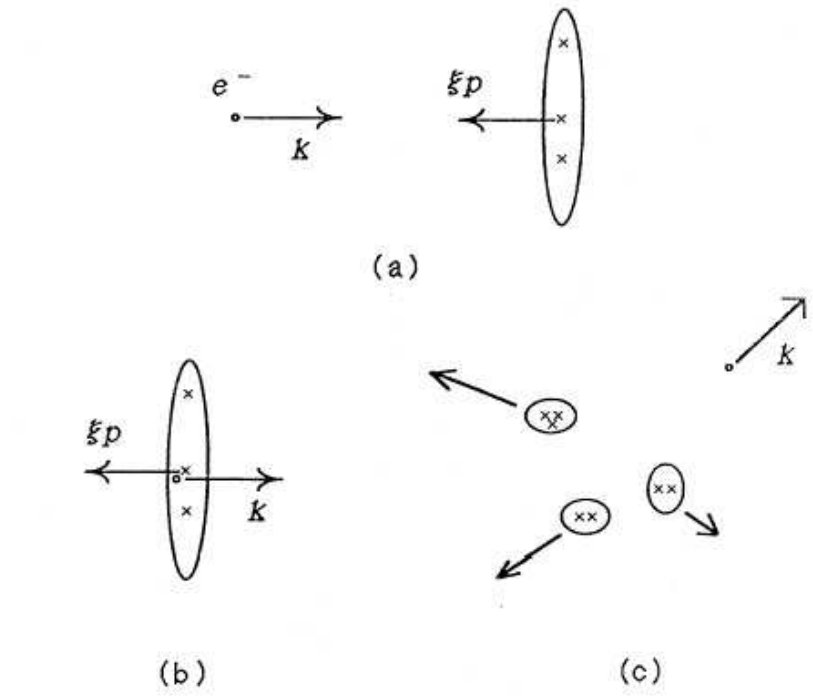

Figure 2.3: The schematics of electron-hadron scattering[3]

The system before scattering in cms consists of a point-like electron and a hadron with four-momentum p. The hadron can be seen as a set of partons in some virtual state of definite fractional momentum $\xi_i p$. The virtual state of partons is characterized by a lifetime τ. Let's suppose that there is a lower bound so that the hadron is made up primarily of virtual states of nonzero lifetime. Now, the Lorentz contradiction and time dilatation can be added to our calculation. Therefore, the lifetime of a virtual state increases to $\tau(1-\frac{v^2}{c^2})^{-\frac{1}{2}} >> \tau$ and the distance for the electron to pass through hadron decreases similarly. As the energy of collision goes to infinity, the time it takes the electron to cross the hadron goes to zero. So at the time of collision the electron sees a set of partons that are effectively frozen for the time of passage[3]. Assuming that partons are randomly spread out over hadron, the probability of finding

additional parton near one parton scattering that can join the scattering is suppressed by $\frac{1}{Q^2 \pi R_0^2}$, where R_0 is the radius of hadron. Therefore the whole system simplifies to the system where one point-like particle scatters on another point-like particle(parton) which is almost at rest. Therefore the cross-section is given by the probability of finding a single parton with given momentum fraction times the cross-section of the electron-parton interaction. After the interaction, the fragments hadronizes. The time it takes is also long compared with the collision, therefore the process of hadronization happens too late to influence the scattering itself. So, the elastic Born approximation can be used to solve the electron-parton scattering.

2.4 Calculation of partonic cross-sections in hadron collisions

Here we will outline the perturbative approaches used to calculate hard scattering processes and describe some of their features and limitations.

2.4.1 Leading-order calculations

The simplest prediction is to calculate the lowest order in the perturbative expansion of the observable. This is performed by calculating the squared matrix element represented by Feynman diagrams and integrating this over the appropriate phase space. For some simple processes and certain observables this can be done analytically. However, to obtain fully differential predictions in general, the calculation must be done numerically. Mostly it is necessary to impose restrictions on the phase space in order that divergences in matrix elements are avoided. Let's see the W+1 jet production calculation

W+1 jet production

Let's have a Drell-Yan W production. We will extend the LO diagram by adding a final state gluon to each of the initial state quark legs

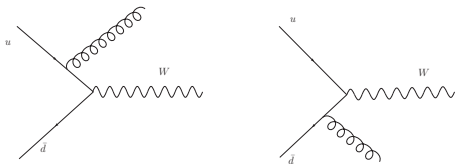

Figure 2.4: Feynman diagrams for W+1 production

to produce W+1 jets (one of sub-processes leading to W+1 jets). The other crossed process is $gq \rightarrow Wq$. Square matrix elements obtained from the sum of the diagrams is[2]

$$|\mathfrak{M}_{u\bar{d}\to Wg}|^2 \sim (\frac{\hat{t}^2+\hat{u}^2+2Q^2\hat{s}}{\hat{t}\hat{u}})$$

where Q^2 is the virtuality of the W boson, $\hat{s} = s_{u\bar{d}}$, $\hat{t} = s_{ug}$, $\hat{u} = s_{\bar{d}g}$. This expression diverges in the limit, where the gluon is unresolved - it is collinear to one of the quarks ($\hat{t} \to 0$ or $\hat{u} \to 0$) or it is soft ($E_g \to 0$). Let's analyze how these divergences can be avoided.
To calculate the cross-section, we must convolute pdfs with our results(see Factorization theorem) and perform the integration over the appropriate phase space

$$\sigma = \int dx_1 dx_2 f_u(x_1,Q^2) f_{\bar{d}}(x_2,Q^2) \frac{|\mathfrak{M}|^2}{32\pi^2\hat{s}} \frac{d^3p_W}{E_W} \frac{d^3p_g}{E_g} \delta(p_u + p_{\bar{d}} - p_g - p_W)$$

where x_1,x_2 are momentum fractions of the u and $\bar{d}$ quarks. This can be written in the form of a cross-section differential in Q^2,p_T and rapidity y of the W boson

$$\frac{d\sigma}{dQ^2 dy dp_T^2} \sim \frac{1}{s} \int_{gluon\ rapidity} dy_g f_u(x_1,Q^2) f_{\bar{d}}(x_2,Q^2) \frac{|\mathfrak{M}|^2}{\hat{s}}$$

The p_T of the gluon is related to Mandelstam variables(invariants) by $p_T^2 = \frac{\hat{t}\hat{u}}{\hat{s}}$. Thus the leading divergence ($\sim \frac{2Q^2\hat{s}}{\hat{t}\hat{u}} = \frac{2Q^2}{p_T^2}$), assuming $\hat{t} \to 0$,$\hat{u} \to 0$ and the gluon is soft, can be written as $\frac{1}{p_T^2}$. Furthermore, for $\hat{s} \to Q^2$

$$\frac{d\sigma}{dQ^2 dy dp_T^2} \sim \frac{2}{s}\frac{1}{p_T^2} \int dy_g f_u(x_1,Q^2) f_{\bar{d}}(x_2,Q^2) \ + \ \text{sub} - \text{leading in } \mathrm{p_T}$$

As the p_T becomes small, the limits on the y_g integration are given by $\pm log\frac{\sqrt{s}}{p_T}$. Let's assume that the rest of the integrand is approximately constant, the integral is[2]

$$\frac{d\sigma}{dQ^2 dy dp_T^2} \sim \frac{log(\frac{s}{p_T^2})}{p_T^2},$$

so the differential cross-section contains logarithmic dependence on $\frac{1}{p_T^2}$. If no cut is applied on the gluon p_T, the integral over p_T diverges. Only when we apply a cutoff at $p_T = p_{Tmin}$, the result is proportional to $log^2(\frac{s}{p_{Tmin}^2})$(after integration over p_T). For very small values of p_T, we can assume the radiated gluon being emitted from the quark line at an early time ("initial state radiation"). This radiation is indeed produced for large rapidities and it is found in the forward region. There is a collinear pole in the matrix element so that a fixed energy gluon tends to be emitted close to the original parton direction . However, we want rather fixed transverse momentum. Using a higher p_T cutoff

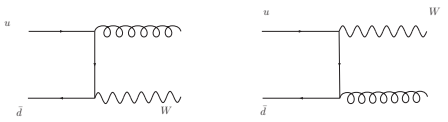

Figure 2.5: Feynman diagrams for W+1 production as 2→2 scattering

the gluon is emitted less often at large rapidities. In our case, we can instead think of the diagrams as a $2 \to 2$ scattering.

There is also a collinear pole involved for the emission of gluons from final state partons. Thus, gluons will be emitted preferentially near the direction of the emitting parton.

W+2 jet production

By adding a further parton, the production of a W+2 jet final state can be simulated. In general many different partonic processes contribute but we just consider the production of a W boson in association with two gluons. In the limit that one of the gluons(p_1) is soft, singularities in matrix elements occur in four diagrams only

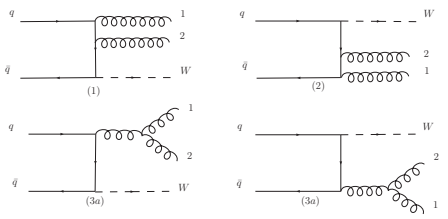

Figure 2.6: Feynman diagrams for W+2 production

Remaining diagrams, where the gluon p_1 is attached to an internal line, do not make any singularities, because the adjacent propagator does not vanish in this limit. But here matrix elements contain also a non-trivial colour structure. Let's denote the colour labels of gluons p_1 and p_2 as t^A and t^B respectively. In such case, the first diagram is proportional to $t^B t^A$ and the second is proportional to $t^A t^B$. Final two diagrams are each proportional to $f^{ABC} t^C$, which can be written as $t^A t^B - t^B t^A$. Using this identity, the amplitude (p_1 soft) can be written with the dependence on the colour matrices factored out[2]

$$\mathfrak{M}_{q\bar{q}\to Wgg} = t^A t^B (D_2 + D_3) + t^B t^A (D_1 - D_3).$$

The terms D_i contain the kinematic structure from Feynman rules. This combination is often called colour-ordered amplitudes. Now, we can square the

amplitude using identities $tr(t^A t^B t^B t^A) = NC_F^2$ and $tr(t^A t^B t^A t^B) = -\frac{C_F}{2}$ to [2]

$$|\mathfrak{M}_{q\bar{q}\to Wgg}|^2 = NC_F^2[|D_2 + D_3|^2 + |D_1 - D_3|^2] - C_F \mathrm{Re}[(\mathrm{D}_2 + \mathrm{D}_3)(\mathrm{D}_1 - \mathrm{D}_3)^\star] = \\ = \frac{C_F N^2}{2}[|D_2 + D_3|^2 + |D_1 - D_3|^2 - \frac{1}{N^2}|D_1 + D_3|^2]$$

These colour-ordered amplitudes possess special factorization properties in the limit that gluon p_1 is soft. They can be written as the product of special term and matrix elements containing only one gluon

$$D_2 + D_3 \;\to\; \epsilon_\mu(\frac{q^\mu}{p_1 q} - \frac{p_2^\mu}{p_1 p_2})\mathfrak{M}_{q\bar{q}\to Wg}$$
$$D_1 - D_3 \;\to\; \epsilon_\mu(\frac{p_2^\mu}{p_1 p_2} - \frac{\bar{q}^\mu}{p_1 \bar{q}})\mathfrak{M}_{q\bar{q}\to Wg}$$

where ϵ_μ is the polarization vector for gluon p_1. The square of these terms are easily computed using the replacement $\epsilon_\mu \epsilon_\nu \to -g_{\mu\nu}$ to sum over gluon polarizations. Let's denote the form

$$\frac{ab}{p_1 a p_1 b} =: [a\ b].$$

The final result is

$$|\mathfrak{M}_{q\bar{q}\to Wgg}|^2 \xrightarrow{\text{soft}} \frac{C_F N^2}{2}[[q\ p_2] + [p_2\ \bar{q}] - \frac{1}{N^2}[q\ \bar{q}]]\mathfrak{M}_{q\bar{q}\to Wg}$$

The leading term contains singularities along two lines of colour flow - one connecting the gluon p_2 to the quark, the other connecting it to the antiquark. The sub-leading terms has singularities along the line connecting the quark to antiquark. This lines indicate preferred directions for the emission of additional gluons. In the sub-leading term the colour flow does not relate the gluon colour to parent quarks at all. The matrix elements are exactly the same as those for the emission of two photons from a quark line. Since all partons are massless, it is easy to rewrite D factors in terms of the energy of the radiated gluon(E) and the angle it makes with the hard partons (Θ_a, Θ_b). It can be combined with the phase space for the emitted gluon which yields to a contribution such as

$$[a\ b]dPS_{gluon} = \frac{1}{E^2}\frac{1}{1-\cos\Theta_a} E\ dE\ d\cos\Theta_a.$$

From that it is clear that the cross-section diverges at $\cos\Theta_a \to 1$(gluon emitted collinear to parton) or $E \to 0$. Furthermore, each divergence is logarithmic. If we regulate divergences by providing a fixed cutoff, it will produce two logarithms(from collinear configuration and from soft processes). This argument can be applied at successively higher orders of perturbation theory. Each

gluon, added to the diagram, yields an additional power of α_S and can produce additional two logarithms. We can rewrite the W+1 jet cross-section as a sum of contribution

$$d\sigma = \sigma_0(W{+}1\ jet)[1{+}\alpha_S(c_{12}L^2{+}c_{11}L{+}c_{10}){+}\alpha_S^2(c_{24}L^4{+}c_{23}L^3{+}c_{22}L^2{+}c_{21}L{+}c_{20}){+}\alpha_S^3\dots]$$

where L represents the logarithm controlling the divergence(soft or collinear). The size of L depends upon the criteria used to define jets - minimum transverse energy of the jet and the jet cone size. Coefficients c_{ij} depend on colour factors. The addition of each gluon results not just in an additional factor of α_S but in $\alpha_S \times \log$. These logarithms can be large, leading to an enhanced probability for additional gluon emissions to occur. Let's rewrite the expansion in brackets as

$$[\quad] = 1{+}\alpha_S L^2 c_{12}{+}(\alpha_S L^2)^2 c_{24}{+}\alpha_S L c_{11}(1{+}\alpha_S L^2 \frac{c_{23}}{c_{11}}{+}\dots){+}\cdots = e^{[c_{12}\alpha_S L^2 + c_{11}\alpha_S L]}$$

The first term in the exponent is referred as the leading logarithmic term. The second term is needed for reproducing NLO logarithms. This reorganization of perturbative expansion is useful when the product $\alpha_S L$ is large. Furthermore, it is basis for all order predictions and it can be interpreted in terms of Sudakov probabilities.

2.4.2 Next-to-leading-order calculations

Although LO calculations can describe broad features of a particular process and provide the first estimate of its cross-section, in many cases this approximation is insufficient. The inherent uncertainty in a lowest order calculation derives from its dependence on the unphysical renormalization and factorization scale, which is often large. In addition, some processes may contain large logarithms that need to be resumed. Some extra partonic processes may contribute only when going beyond the first approximation. A NLO QCD calculation needs to consider all diagrams that contribute additional strong coupling factors α_S. They can be constructed from LO ones by adding additional quarks and gluons. They can be divided into two categories - virtual(loop) contributions and the real radiation component. At first, let's take the virtual contributions

In order to evaluate such diagrams, we have to introduce an additional loop momentum l, that circulates around the loop and is unconstrained. Therefore it is necessary to integrate over the momentum l. However, the resulting contribution is not finite but contains infrared divergencies. In order to isolate singularities, it can be analyzed, that divergencies in each contribution are equal with opposite sign and the result is finite. The real contribution consist of LO W+1 jet production diagrams together with a quark-gluon scattering piece which can be obtained from these diagrams by interchanging the gluon in the final state with a quark(antiquark) in the final state. But the $q - \bar{q}$ matrix elements contain a singularity as the gluon $p_T \to 0$. Therefore, we have to regulate and then isolate these singularities to obtain finite prediction for $p_T \to 0$.

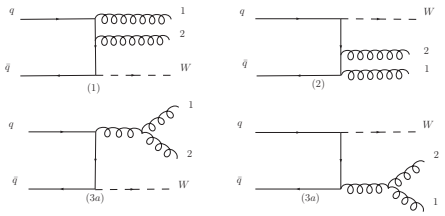

Figure 2.7: Feynman diagrams NLO approximation

The most common method to do so is the dimensional regularization. This approach consists of extending the number of dimensions to D=4+2ϵ;$\epsilon > 0$. Now (in intermedial stages) the singularities appear as single and double poles in ϵ. After they have canceled, the limit $\epsilon \to 0$ sets the right dimension. Let's see it schematically. Consider a calculation

$$I = \lim_{\epsilon \to 0}(\int_0^1 \frac{dx}{x} x^{-\epsilon} \mathfrak{M}_{(x)} + \frac{1}{\epsilon}\mathfrak{M}_{(0)}),$$

where $\mathfrak{M}_{(x)}$ is the real radiation matrix element integrated over the extra phase space of the gluon emission, which contains a regulating factor $x^{-\epsilon}$[2]. The variable x represents a kinematic invariant that vanishes as the gluon becomes unresolved. The second term represents the virtual contribution which contains an explicit pole $\frac{1}{\epsilon}$ times the LO matrix element $\mathfrak{M}_{(0)}$. We can use two techniques for isolating singularities - substraction method and phase space slicing. Let's stick to the former one. Now, we explicitly add and subtract the divergent term, such that the new radiation integral is manifestly finite

$$I = \lim_{\epsilon \to 0}(\int_0^1 \frac{dx}{x} x^{-\epsilon}[\mathfrak{M}_{(x)} - \mathfrak{M}_{(0)}] + \mathfrak{M}_{(0)} \int_0^1 \frac{dx}{x} x^{-\epsilon} + \frac{1}{\epsilon}\mathfrak{M}_{(0)}) = \int_0^1 \frac{dx}{x}[\mathfrak{M}_{(x)} - \mathfrak{M}_{(0)}]$$

This can be generalized to render finite real radiation contribution to any process with a separate counter-term for each singular region of phase space. The inclusion of real radiation diagrams in a NLO calculation extends the range of predictions that may be described by a LO calculation. For W boson the production leads to zero p_T at LO, but it acquires finite p_T at NLO. Even then, the W p_T is exactly balanced by p_T of a single parton. In a real event, the W p_T is typically balanced by the sum of several jet p_T. In a fixed order calculation, these contributions would be included by moving to even higher orders so that configurations, where the W p_T is balanced by two jets enter at NNLO.

NLO K-factor

The K-factor is a useful shorthand which shows the strength of the NLO corrections to the LO cross-section. It can be calculated by taking the ratio of NLO and LO cross-section. The K-factor may considerably differ from various kinematic regions of the same process, but in practice, the K-factor often varies

slowly and may be approximated with one number[2]. The ratio depends quite strongly on pdfs used in NLO/LO evaluations. Now, it is standard practice to use a NLO pdf when evaluating the NLO cross-section and a LO pdf for the LO cross-section. But sometimes the same pdf set can be used for both predictions. Some complications can arise from the fact that K-factor depends significantly on the region of phase space that is being studied. If we have to apply some cutoff to obtain finite cross-section, the K-factor again depends upon the value of this cut. Lastly, the K-factor depends upon the renormalization and factorization scales at which it is evaluated. A K-factor can be less than, equal to, or greater than 1, depending on all of the factors above. Such K-factors can be used as estimators for the NLO corrections for processes in situation, where only the LO cross-sections are available.

2.4.3 Next-to-next-to-leading-order calculations

Considering a NLO approximation, it is natural to move deeper into the perturbation expansion. Furthermore, the first meaningful estimate of the theoretical error of any reliable prediction of an observable at NLO if we go to NNLO. A further reduction of scale uncertainties is expected and in cases where NLO corrections are large, it is a chance to check the convergence of the perturbative expansion. However, the NNLO calculation needs more numerous and more complicated approach than NLO[2]. Different contributions can best be understood by considering all possible cuts of a $O_{(\alpha_S^3)}$ three-loop diagram. The first contribution corresponds to 2-loop 3-parton diagrams. The second contribution corresponds to the square of the 1-loop 3-parton matrix elements. The third contribution also contains one loop matrix elements but with 4 partons in the final state. One of them is unresolved. As in NLO calculation, each unresolved parton produces a divergent contribution. The final contribution involves only tree-level 5-parton matrix elements. This piece contains two unresolved partons and this gives rise to singularities that must be subtracted. However, at present, no general procedure for doing this exists. Such calculation represents the current frontier of NNLO predictions. For processes as $2 \rightarrow 1$ and $2 \rightarrow 2$, NNLO results are already available. The total inclusive cross-section at NNLO is known for processes such as Drell-Yan production via W or Z bosons, Higgs boson production(one scale problem in the limit of large m_T). For both processes, NLO corrections are very large, but NNLO terms provide only a small increase. The calculations have now been extended to include rapidity cuts on leptons in Drell-Yan process.

2.4.4 All orders approach

Rather than systematically calculating to higher and higher orders in the perturbative expansion, a number of "all-orders" approaches are used to describe phenomena observed at high-energy colliders. Resummation is one such approach - dominant contributions from each order in PT are singled out and resumed by the evolution equation. Near boundaries of phase space, fixed order

predictions break down due to large logarithmic corrections. For example, the expression for the W boson p_T where leading logarithms have been resumed to all orders is given by[2]

$$\frac{d\sigma}{dp_T^2} = \sigma \frac{d}{dp_T^2} e^{(-\frac{\alpha_S C_F}{2\pi} \log^2 \frac{M_W^2}{p_T^2})}$$

Note that in this approximation the p_T^2 distribution vanishes as $p_T \to 0$. This feature is, however, not seen experimentally. A different approach is provided by parton showers. Using the parton showering process, a few partons produced in a hard interaction at high energy scale can be related to partons at an energy scale close to Λ_{QCD}. At this lower energy scale a universal non-perturbative model can be used to provide the transition from partons to the hadrons that are observed experimentally. This is possible because the parton showering allows using DGLAP formalism for evolution of the parton fragmentation function. The solution of DGLAP evolution equation can be rewritten using Sudakov form factors[2]. That indicates the probability of evolving from a higher scale to a lower scale without the emission of a gluon greater than a given value. For the case of parton showers from the initial state, the evolution proceeds backwards from the hard scale to the cutoff scale with Sudakov form factors weighted by parton distribution functions. In parton showering process, successive values of an evolution variable t, momentum fraction z and an azimuthal angle Φ are generated along with flavours of partons emitted during the showering. The evolution variable t can be the virtuality of the parent parton, $E^2(1-\cos\Theta)$ [E being the energy of parent parton and Θ being the angle between partons] or the square of the relative p_T of two partons. Note that with parton showering, we introduce two new scales, one for initial state parton showering and one in the final state. The expression for Sudakov form factor of an initial state parton is in the form

$$\Delta_{(t)} := e^{(-\int_{t_0}^{t} \frac{dt'}{t'} \int \frac{dz}{z} \frac{\alpha_S}{2\pi} P_{(z)} \frac{f_{(x/z,t)}}{f_{(x,t)}})}$$

where t is the hard scale, t_0 is the cutoff scale and $P_{(z)}$ is the splitting function for the branching under consideration. The Sudakov form factor has a similar form for the final state but without pdfs weighting. The introduction of the Sudakov form factor resums all the effects of soft and collinear gluon emission, which leads to well-defined predictions even in this region. The Sudakov form factors give the probability for a parton to evolve from a harder scale to a softer scale without emitting a parton harder than some resolution scale, either in the initial state or in the final state. A Sudakov form factor will depend on the parton type, the momentum fraction x of the initial state parton, the hard and cutoff scales for the process and the resolution scale for the emission.

2.4.5 Parton distribution functions

The calculation of production cross-sections at hadron colliders relies upon a knowledge of the distribution of the momentum fraction x of partons in proton

in the relevant kinematic range. These parton distribution functions cannot be calculated perturbatively, but rather are determined by global fits to data from the deep inelastic scattering, Drell-Yan and jet production. Measurements of deep inelastic scattering structure functions (F_2, F_3) in the lepton-hadron scattering and of lepton pair production cross-sections in hadron-hadron collisions provide the main source on quark distributions $f_{p\to q}(x, Q)$ inside hadrons. At LO, the gluon distribution function $f_{p\to g}(x, Q)$ enters directly in hadron-hadron scattering processes with jet final states. Recent global parton distribution fits are carried out to NLO and in some cases to NNLO, which allows $\alpha_S(Q^2)$,$f_{p\to q}(x, Q)$ and $f_{p\to g}(x, Q)$ to mix and contribute in the theoretical formulae for all processes. Data from deep inelastic scattering, Drell-Yan and jet processes utilized in pdf fits cover a wide range in x and Q. The DGLAP-based NLO pQCD should provide an accurate description of the data(and of the evolution of the parton distributions) over the entire kinematic range present in current global fits. There is a remarkable consistency between data in pdf fits and the pQCD theory fit to them. For most of data points, statistical errors are smaller than systematic errors, so a proper treatment of systematic errors and their bin-to-bin correlations is important. The accuracy of the extrapolation to higher Q^2 depends on the accuracy of the original measurement, uncertainty on $\alpha_S(Q^2)$ and the accuracy of the evolution code. Most global pdf analysis are carried out at NLO. The DGLAP evolution kernels have been calculated at NNLO and so NNLO pdfs calculated in this manner are available. However, any current NNLO global pdf analysis are still approximative. All global analysis use a generic form for the parametrization of both the quark and gluon distributions at some reference value Q_0[2]

$$F(x, Q_0) = A_0 x^{A_1}(1-x)^{A_2} P(x, A_3 \dots).$$

The reference value Q_0 is usually chosen in the range of 1-2GeV. The parameter A_1 is associated with small-x Regge behaviour while A_2 is associated with the large-x valence counting rules. The term $P(x, A_3 \dots)$ is a suitably chosen smooth function, depending on one or more parameters, that adds more flexibility to the pdf parametrization.

2.5 Drell-Yan pair production cross-section calculation

The Drell-Yan production in hadronic collisions yields complementary information as from deep inelastic or electron-positron collisions. Since the lepton pair have no direct interactions with hadrons, they provide a clear signal of the production of virtual gauge particles $\gamma, W^{\pm}, Z^0$, which couples to them via electroweak force. The intermediate bosons $W^{\pm}, Z^0$ can also be physical, when the cms energy is large enough. Let's start with Drell-Yan production via virtual photon

$$A_{(p)} + B_{(p')} \rightarrow \gamma^{\star}_{(q)} + X \rightarrow l_{(k)} + l'_{(k')} + X$$

where X are the hadronic fractions(in final state) that do not contribute to the high p_T process. If we denote $q = k' + k$ the total momentum of the lepton pair, then the invariant mass of lepton pair is

$$q^2 = M^2 c^2$$

Furthermore, the virtual photon is timelike, so $q^2 = Q^2 > 0$. Let's introduce a scaling variable $\tau = \frac{q^2}{s}$, where s is a Mandelstam cms energy. Using the factorization theorem[3]

$$\frac{d\sigma_{AB}(p,p',q)}{dq^2} = \sum_f \int_0^1 dx_1 dx_2 f_{f/A}(x_1) \frac{d\sigma_{f\bar{f}}}{dq^2} f_{\bar{f}/B}(x_2)$$

where $f_{f/A}$ and $f_{\bar{f}/B}$ are parton distribution functions from the deep inelastic scattering. The hard scattering is the Born approximation for $q\bar{q}$ annihilation into virtual photon, averaged over colour degrees of freedom.

$$\frac{d\sigma_{f\bar{f}}}{dq^2} = Q_f^2 \frac{4\pi\alpha^2}{3N_c q^2} \delta(q^2 - (x_1 p + x_2 p')^2)$$

If we introduce our scaling, we have

$$\frac{d\sigma_{AB}(p,p',q)}{dq^2} = \frac{4\pi\alpha^2}{3N_c q^2 s} \sum_f Q_f^2 \int_0^1 dx_1 dx_2 f_{f/A}(x_1) \delta(\tau - x_1 x_2) f_{\bar{f}/B}(x_2)$$

For other intermediate bosons we have

$$\frac{d\sigma_{AB}^{(\gamma,W,Z)}(p,p',q)}{dq^2} = \sigma_0^{(\gamma,W,Z)}(q^2) W_{AB}^{(\gamma,W,Z)}(\tau)$$

where σ_0 contains overall dimensions and the dimensionless function W_{AB} is

$$W_{AB}(\tau) = \int_0^1 dx_1 \int_0^1 dx_2 \delta(\tau - x_1 x_2) D_{AB}(x_1, x_2)$$

In the case of Z boson

$$\sigma_0^Z = \tau \frac{\pi\alpha^2}{192 N_c \sin^4\Theta_W \cos^4\Theta_W} \frac{1 + (1 - 4\sin^2\Theta_W)^2}{(q^2 - M_Z^2)^2 + M_Z^2 \Gamma_Z^2}$$

where

$$\Gamma_Z = \frac{\alpha M_Z}{24 \sin^2\Theta_W \cos^2\Theta_W} (1 - 4\sin^2\Theta_W + 8\sin^4\Theta_W)$$

is the total width of Z boson. The relevant product of distributions is

$$D^Z_{AB}(x_1, x_2) = \sum_q C_q(f_{q/A}(x_1)f_{\bar{q}/B}(x_2) + f_{\bar{q}/A}(x_1)f_{q/B}(x_2))$$

and

$$C_q = 1 + (1 - 4|Q_q| \sin^2 \Theta_W)^2$$

The total Z boson production cross-section is found by integrating over q^2 in the narrow-width approximation $\Gamma_Z << M_Z$[3]

$$\sigma^{(Z)}_{tot} = \frac{\pi^2 \alpha_S}{12s \sin^2 \Theta_W \cos^2 \Theta_W} W_Z(\tau = \frac{M_Z^2}{s}, q^2 = M_Z^2).$$

Chapter 3

Programs for generating events - Pythia

The program PYTHIA[7] is used for generating high energy physics collisions. Especially it is made to calculate a set of outgoing particles from the interaction between two incoming particles. However, physics of such processes is not understood well enough to calculate it exactly[3]. The program is rather based on a combination of analytical results and QCD-based models. This physics include areas such as hard subprocesses, initial and final state parton showers, beam remnants and underlying events, fragmentation and decays. The emphasis lays on multiparticle production from collisions such as e^+e^-,pp and ep hard interactions. The program is intended to generate complete events up to experimentally observable ones, within our currently known underlying physics. In the first approximation, all processes have a structure of interactions between elementary particles (quarks, leptons, gauge particles). Corrections to this approach can be divided into three main classes[7].

- Bremsstrahlung-type modifications - emission of additional final state particles. Especially the emission via the strong force is potent because of the largeness of the α_S. We therefore speak about "parton showers", which means that a single parton may give rise to a whole bunch of partons in the final state. Bremsstrahlung corrections do not depend on details of the process studied, but only on few key numbers, such as the momentum transfer scale. Such universal corrections can be included through probability to arbitrarily high orders. Alternatively, exact calculations of bremsstrahlung can be carried out order by order in perturbation theory. But this can be done up to few orders because of the complexity of calculations.

- "True" high order corrections - combination of loop graphs and soft parts of the bremsstrahlung graphs. This combination is needed to cancel some divergencies. Necessary perturbative calculations are usually very difficult

and contain only one loop.

- Confinement of quarks and gluons - in previous points we have used a perturbative approach to describe short-distance interactions of quarks, leptons and gauge bosons. For leptons and colourless bosons this approach is sufficient. For quarks and gluons it has to be complemented with the structure of incoming hadrons for hadronization process. The hadronization can be further divided into fragmentation and decays. The former describes the way the creation of new quark-antiquark pairs can build hadrons. This process is still not yet fully understood.

The structure of interaction now consist of hundreds of final state particles instead of two. The analysis of such complicated model has to be solved numerically using an event generator. In an event generator, computers are used to generate events as detailed as could be observed by a perfect detector. This is not done in one step, but rather by factorizing the full problem into a number of components of reasonable difficulty. This means that the hard process is used as the input to generated bremsstrahlung corrections and the result of this calculation is then left to hadronize. The output of an event generator should be in the form of "events" with the same behavior and the same fluctuations as real data[7]. In data, fluctuations arise from the quantum mechanics of the underlying theory. In generators, Monte Carlo techniques are used to select all relevant variables according to the desired probability distributions and therefore ensure randomness in final events. Let's try to follow the evolution of an event in some prompt of a time order.

- Two particles are coming into the collision. Each of them is characterized by a set of pdfs that define its substructure.
- One parton from each of particles starts off a sequence of branchings which build up an initial state shower.
- One parton from each of particles enters the hard process which produces a number of outgoing particles. This part gives the character to the event.
- The hard process may produce a set of short-lived resonances ($Z^0, W^{\pm}, \ldots$), which later decay to normal partons.
- Outgoing partons may branch to build up final state showers.
- In addition to the hard process some semi-hard interactions may occur between other partons of incoming particles.
- QCD confinement mechanism starts the hadronization to colour neutral hadrons.
- Many of produced hadrons are unstable and decay further.

Conventionally, only quarks and gluons are counted as partons. These points describes well an interaction between two leptons, lepton and hadron and two hadrons. Let's study further some of points above. The current PYTHIA contains around 240 different hard processes. The classification can be done according to the number of final state objects : $2 \to 1$, $2 \to 2$, $2 \to 3$ etc. PYTHIA is optimized for $2 \to 1$ and $2 \to 2$ processes, because there is no generic treatment for three particles in the final state. We can clasify processes according to the physics scenario:

- hard QCD
- soft QCD(diffractive, elastic scattering, minimum bias event)
- heavy flavour production
- prompt photon production($qg \to q\gamma$)
- photon induced process($\gamma q \to q\bar{q}$)
- deep inelastic scattering($lq \to lq$)
- W/Z boson production
- SM Higgs mechanism
- Gauge boson scattering processes
- non-SM Higgs production
- production of new gauge bosons
- technicolour production
- supersymetry production
- several other approaches - compositenes, left-right symetric models, leptoquark production

Within these physics not all contributing graphs have been included. Also in many cases various approximations were used for the matrix element calculation. The bulk of processes above are $2 \to 2$ kind and very few of them leads to more than 2 final state particles. The classification may also be misleading since an s-channel resonance is considered as a single particle, even if it always decays to two final-state particles. Decay chains can become quite long, but follow a straight perturbative pattern. If the simulation is restricted to only some set of decays, the corresponding cross-section reduction can be calculated. The decay products of resonances are typically quarks, leptons or other resonances. Hadrons are produced in hadronization phase. In decays to quarks, parton showers are added to give more realistic multijet structure. Also the photon emission off leptons may be allowed. In every process that contains coloured or charged objects in initial or final state the gluon or photon emission may give

large corrections to the topology of event. As the available energy increases, hard emission of this kind increases in importance relative to fragmentation. Two traditional approaches exist to the modeling of perturbative corrections[3]. One is the matrix element method (Feynman diagrams order by order). Second is the parton shower one. In principle, the former one is the correct approach that takes into account exact kinematics, full interference and helicity structure. The only problem is that calculations are almost impossible for higher orders, especially with loop graphs. In the latter case an arbitrary number of branchings of one parton into several ones may be combined to yield a description of multijet events with no explicit upper limit on the number of partons involved. This is due to the fact that approximations from simplified kinematics, interference and helicity structure is used rather than full matrix element. However, because of its simplicity and flexibility, this choice is used primarily and the other approach is used only for α_S determinations, angular distribution of jets, triple gluon vertex studies and so on.

Chapter 4

ATLAS physics overview

The Large Hadron Collider offers a large range of physics opportunities. The ATLAS detector should reflect the need to be sensitive to many physics phenomena. The most important goal is to probe the origin of the electroweak scale, mainly the existence of the Higgs boson[5][6]. This search will be followed by looking for other phenomena related to the symmetry breaking - particles from supersymmetry and technicolor theories, new gauge bosons and composite quarks and leptons. Second important component of the ATLAS physics programme is the investigation of CP violation in B decays and the measurement of W and top masses[2]. The supersymmetry is a concept for which there is no experimental evidence. It incorporates (as the only theory so far known) gravity into the quantum theory of particle interactions. Also it offers a cancelation mechanism for the divergencies, assuming that the theory is supersymmetric at the electroweak scale. Some supersymmetric models even allow for the unification of gauge couplings at a high scale. This should decrease the number of parameters in the theory as a whole. The only particle, which is incorporated in the Standard model and is jet unobserved is one physical scalar Higgs particle (composed of two scalar fields). Supersymmetric models postulate the existence of many superpartners - bosonic superpartners for fermions, fermionic ones for bosons and multiple Higgs bosons h,H,A,$H^{\pm}$. This is one of the big objective of ATLAS experiment. Parameters of supersymmetric models are jet unknown so precise measurement of masses, decay rates and couplings will be another part of physical analysis. For the strong coupling there exists a technicolor scenario for models based on dynamical symmetry breaking. It may have something to do with the electroweak symmetry breaking. Both two theories if they could explain the electroweak symmetry breaking, should have masses of proper particles in 1 TeV region. There are also other possibilities for new physics, not necessarily related to the scale of the electroweak symmetry breaking. There could be new neutral or charged bosons with a mass larger than Z and W bosons, also new quarks, charged leptons or massive neutrinos. There is also possibility, that quarks and leptons are not elementary particles.

4.1 QCD processes at the LHC

Even at low luminosity phase, ATLAS will be a great tool for measuring QCD processes with high statistics in large energy regime. It is of particular interest to study jet and photon physics, open charm, open beauty and gauge bosons production. Mainly the diffractive processes and production of jets, gauge bosons and heavy flavour partons will be studied in details[6]. The exploration of the hard partonic processes will be extent to the order of hundreds GeV^2 in energy scale while reaching the fraction momentum of the proton being carried by a scattered protons to the order of 10^{-5}. The measurement of Drell-Yan process, W bosons, Z boson, photons, high-p_T jets and heavy flavours production will serve to derive the partonic distribution function. Even the deviation from theoretical predictions for QCD events themselves will indicate the existence of new physics. It will be especially important to measure precise parameters of QCD such as coupling constant and masses of intermediate particles. Extending our knowledge in QCD will increase the precision in the calculation of production cross-section of almost all processes as they are controlled by QCD. Main tests of QCD will be made by comparing measurements to LO or NLO calculations or to leading-log Monte Carlo programs, which contain $2 \leftarrow 2$ LO matrix elements and approximate higher orders through parton showers[6]. The difference between a LO and NLO calculation is quantified in the K-factor

$$Kfactor = \frac{\sigma_{NLO}}{\sigma_{LO}}.$$

K factor can be higher than 1, especially when new sub-processes appear at the next-to-leading order.

4.1.1 Drell-Yan physics

For the topic of this research work, the most important part is a Drell-Yan pair production. The Drell-Yan process is a production of a particle-antiparticle pair from intermediate γ^* photon, which comes from $q\bar{q}$ annihilation. We can generalize this process to other intermediate bosons Z,W.

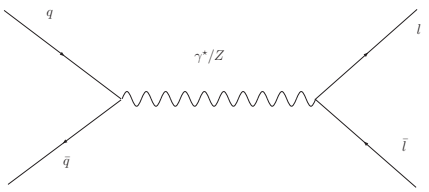

Figure 4.1: Feynmann diagram of Drell-Yan process

This process can probe the proton structure at a scale Q^2 equal to the mass squared of the lepton pair. In pp collisions, Drell-Yan production proceeds

via γ^*/Z bosons and starts from a combination of a valence quark and a sea quark (or from a $q\bar{q}$ both from the sea) with the same flavour. In case of W intermediation this $q\bar{q}$ pair cannot have the same flavour. QCD affects the cross-section for this production only in the initial state. In general valence and sea quarks carries different average momentum fraction. In most cases an asymmetric configuration will be preferred, where one momentum fraction is small and the other large. If we denote them x_1 and x_2, the rapidity of the lepton pair is

$$y = \frac{1}{2} ln \frac{x_1}{x_2}$$

and the invariant mass of the pair is

$$M^2 = x_1 x_2 s$$

If we assume that Drell-Yan pairs can be reconstructed in detector up to rapidities of $2,5$, the maximum ratio possible between two parton momenta is of the order of 150[6]. The measurement of the lepton pair properties (y, M^2) allows us to reconstruct parton momenta and we can therefore guess the parton distribution for quarks. Furthermore, these two leptons are expected to be well separated from jets and other particles. The other advantage of this process is that it can be easily distinguished from background. In case of muons the background can contain directly cosmic rays. Besides that there are two classes of background sources - misidentification of leptons and leptons from heavy quark decays. Both sources will lead to the production of QCD jets and so will not be isolated as Drell-Yan leptons will be. Furthermore, leptons from the Drell-Yan process will have an opposite charge. The expected cross-section will have a resonance contribution due to the production of the Z boson.

The angular distribution of leptons from Drell-Yan processes should be sensitive to effects of non-perturbative QCD. The forward-backward asymmetry of a lepton pair can be used to verify the expected contribution due to the γ^*/Z boson interference for lepton pair masses larger than the Z boson pole. But the presence of heavy neutral gauge bosons can modify the value of the forward-backward asymmetry. For all this and also for kind of nice symmetry in initial and final state, I will stick to the γ^*/Z boson channel. In contrast to jet physics the signature of Drell-Yan lepton pair provides definite identification and there is no final state interactions. In contrast to W boson production, kinematics can be reconstructed accurately since there is no neutrino carrying part of boson momentum. At LHC energies, the cross-section for the Z boson production should have a contribution of more than 10% due to $s\bar{s}$ initial state. The product $x_1 x_2$ is fixed to a value of about 4.10^{-5} at leading order. The main selection method is to be based on triggers requiring two leptons. The cross-section of the Z boson production is at the following graph

The cross-section for quark-antiquark annihilation to a lepton pair via photon(massive) can be obtained even from QED with the addition of the appropriate colour and charge factors[2].

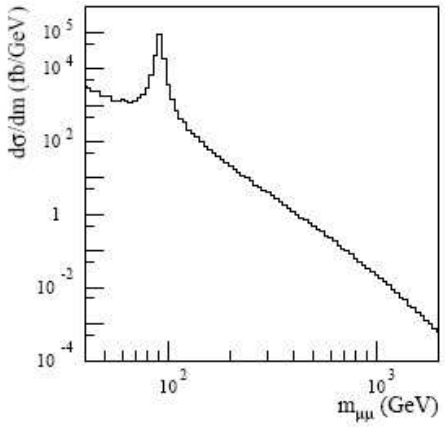

Figure 4.2: Cross-section of Drell-Yan muon production as a function of its invariant mass[6]

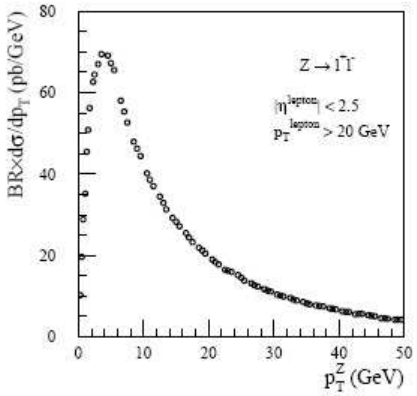

Figure 4.3: The Z boson production cross-section as a function of its transverse momentum[6]

$$\hat{\sigma}(q\bar{q} \to l^+l^-) = \frac{4\pi\alpha^2}{3\hat{s}}\frac{1}{N}Q_q^2$$

where Q_q is a quark charge and $\frac{1}{N}$ is overall colour factor $\frac{1}{3}$. In general, $q\hat{q}$ will have a spectrum of the center-of-mass energies $\sqrt{\hat{s}}$, so it is better to consider differential mass distribution

$$\frac{d\hat{\sigma}}{dM^2_{l^+l^-}} = \frac{\hat{\sigma}_0}{N}Q_q^2\delta(\hat{s} - M^2_{l^+l^-}) \qquad \hat{\sigma}_0 = \frac{4\pi\alpha^2}{3M^2_{l^+l^-}}$$

In the center-of-mass frame, incoming partons momenta are

$$p_1^\mu = \frac{\sqrt{s}}{2}(x_1, 0, 0, x_1)$$
$$p_2^\mu = \frac{\sqrt{s}}{2}(x_2, 0, 0, -x_2)$$

where $\hat{s} = x_1x_2s$. If we use pdfs for initial state quarks and antiquarks in colliding beams, we have

$$\frac{d\sigma}{dM^2_{l^+l^-}} = \frac{\hat{\sigma}_0}{N}\int_0^1 dx_1dx_2\delta(x_1x_2s - M^2_{l^+l^-})\times[\sum_k Q_k^2(q_k(x_1, M^2)\hat{q}_k(x_2, M^2) + q_k(x_2, M^2)\hat{q}_k(x_1, M^2))]$$

If we use the definition of rapidity, we have

$$x_1 = \frac{M}{\sqrt{s}}e^y \qquad x_2 = \frac{M}{\sqrt{s}}e^{-y}.$$

The double differential cross-section is

$$\frac{d\sigma}{dM^2_{l^+l^-}dy} = \frac{\hat{\sigma}_0}{Ns}[\sum_k Q_k^2(q_k(x_1, M^2)\hat{q}_k(x_2, M^2) + q_k(x_2, M^2)\hat{q}_k(x_1, M^2))]$$

In analogy, the subprocess cross-section for (on-shell) W and Z bosons production is

$$\hat{\sigma}_{q\bar{q}\to W} = \frac{\pi}{3}\sqrt{2}G_FM_W^2|V_{qq'}|^2\delta(\hat{s} - M_W^2)$$
$$\hat{\sigma}_{q\bar{q}\to Z} = \frac{\pi}{3}\sqrt{2}G_FM_Z^2(v_q^2 + a_q^2)\delta(\hat{s} - M_Z^2)$$

where $V_{qq'}$ is CKM matrix element and $v_q(a_q)$ is the vector coupling(axial vector coupling) of the Z boson to quarks. These predictions are calculated at LO, NLO and NNLO in PT with renormalization and factorization scales $\mu_F = \mu_R = M_{W,Z}$. The net effect of NLO and NNLO corrections is to increase

the lowest order cross-section by about 25% and 5% respectively. The only theoretical uncertainty in the prediction comes from unknown $O(\alpha_S^3)$ corrections. The parton distributions are being probed in a range $x \sim \frac{M_W}{\sqrt{s}}$, where they are constrained from the deep inelastic scattering and the scale dependence is weak.

For lepton decays, the minimal transverse momentum is of 20 GeV and they have to be produced within $|\eta| < 2,5$ in order to detect them in the inner part of the detector. The lepton pair mass has to be within ±6 GeV of the nominal Z boson mass. Taking this cut, we can obtain the forward-backward asymmetry of lepton pair production as a function of Z boson rapidity. The forward-backward asymmetry is defined as[6]

$$A_{FB} = \frac{\sigma_F - \sigma_B}{\sigma_F + \sigma_B}$$

where

$$\sigma_F = \int_0^1 \frac{d\sigma}{dcos\Theta} dcos\Theta \qquad \sigma_B = \int_{-1}^0 \frac{d\sigma}{dcos\Theta} dcos\Theta.$$

Measurement of the forward-backward asymmetry can be used to precise measurement of the effective Weinberg angle $sin^2\Theta_W$. For this purpose it is necessary to subtract from A_{FB} contributions from background and higher QCD,QED and weak processes.

4.2 Physics of electroweak gauge bosons

Since there will be about 300 millions single W events expected per year, it is presumed to measure electroweak parameters with statistical uncertainty 2 MeV[6]. It will provide large statistics and high center of mass energy to measure the W mass with a precision better than 20 MeV. A large rate of gauge boson pair production enables testing the triple gauge-boson couplings. As the Standard model predicts the gauge cancelation, it will be measured along with possible anomalous couplings made. The most sensitive variables to compare with the Standard model are the transverse momentum spectra of high-p_T photons and reconstructed Z bosons.
Like Drell-Yan pairs, most W and Z bosons are produced with relatively little p_T (in comparison to $M_{W/Z}$). In LO model (colliding partons are assumed to be exactly collinear with colliding beam particles) W and Z bosons are produced with zero p_T. This, however, does not take account of the intrinsic transverse motion of quarks and gluons inside hadrons and even the possibility of generating large p_T by recoil against additional partons. At very small p_T, the intrinsic transverse motion of quarks and gluons inside hadrons cannot be neglected as shows the p_T distribution of Drell-Yan pairs in fixed target pN collisions. The distribution is well parameterized assuming a Gaussian distribution for the intrinsic p_T with $< k_T > \sim 700MeV$[2]. In that data, there is a clear evidence

of a hard, power-law tail which comes from the emission of one or more hard partons

$$q\hat{q} \rightarrow W/Zg$$
$$qg \rightarrow W/Zq$$

In principle, the hard(PT) and intrinsic(NON-PT) contributions can be combined to give a theoretical prediction for all p_T(using a convolution integral in p_T space). More refined prediction will then include NLO perturbative corrections(O(α_S^2)) to the high p_T tail. Some fraction of the O(α_S) and O(α_S^2) contributions could be expected to correspond to distinct W/Z+1 jet and W/Z+2 jet final states. However, the major problem is that $2 \rightarrow 2$ matrix elements are singular when the final state partons become soft or when they are emitted collinear with initial state partons. Furthermore, processes like $q\bar{q} \rightarrow W/Zgg$ are singular when the two final state gluons become collinear. In other words, the lowest order perturbative contribution to the p_T distribution is singular as $p_T \rightarrow 0$ and higher order contributions from processes like $q\bar{q} \rightarrow W/Zgg$ are singular for any p_T. The O(α_S) contribution to the total W cross-section from the process $q\bar{q} \rightarrow Wg$ is singular when $p_T(W) = 0$, but it is exactly canceled by a O(α_S) contribution from a virtual gluon loop correction to $q\bar{q} \rightarrow W$. The net result is the finite NLO contribution to the cross-section.

4.3 B-physics

From the very beginning LHC will produce $b\bar{b}$ pairs at a rate of 10^{12} per year. About one collision in every hundred will produce a b-quark pair. In ATLAS inclusive-muons with 6 GeV p_T threshold will provide a trigger for initial section of B-event[6]. In this inclusive selection, about 25% of the muon trigger events will contain b-quarks. The important aim of the B-physics work is to test the Standard model through precise measurements of B-hadron decays. It will serve to precise elements of CKM matrix and therefore to indicate the existence of new physics. The measurement program will contain mainly precise measurements of CP violation in B-meson decays, measurements of the periods of flavour oscillations in B_s^0 and B_d^0 and measurements of their relative decay rates. Finally, searches for very rare decays (strongly suppressed in the Standard model) will be performed. It could serve as indirect evidence for new physics.

4.4 Heavy quarks and leptons

The top quark is the only known fundamental fermion with a mass on the electroweak scale. As a result it could provide information about the electroweak symmetry breaking sector. It is presumed that LHC will produce 8 million of $t\bar{t}$ pairs for an integrated luminosity of 10 fb^{-1}[6]. It would allow measurement of top quark mass with a precision of 2 GeV. The single top production

should be observable with high statistics. LHC will be a suitable place to search for the possible existence of fourth generation quarks and leptons. About 1000 events/year will produce a quark mass of 900 GeV. There are two possible Feynmann diagrams that can describe heavy quark production at hadron colliders.

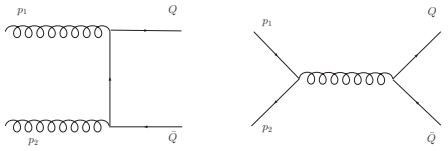

Figure 4.4: Feynman diagrams for heavy quarks production

Unlike for the Drell-Yan process, the total cross-section is sensitive to the gluon content of incoming hadrons as well as the valence and sea quark distributions. The parton distribution functions ar probed at values of

$$x_1 = \frac{m_T}{\sqrt{s}}(e^{yQ} + e^{y\bar{Q}}) \qquad x_2 = \frac{m_T}{\sqrt{s}}(e^{-yQ} + e^{-y\bar{Q}})$$

where $m_T = \sqrt{m_Q^2 + p_T^2}$ is the transverse mass, p_T is the transverse momentum of quarks and $y_Q, y_{\bar{Q}}$ are the quark and antiquark rapidities. The dependence on the quark and gluon pdfs can vary considerably at different cms energies($\sqrt{s}$) and when producing different flavours of heavy quarks. The heavy quark propagator is given by

$$(p_Q - p_1)^2 - m_Q^2 = -2p_Q p_1 = -\sqrt{s}x_1 m_T(\cosh y_Q - \sinh y_Q)$$

which reduces to

$$-m_T^2(1 + e^{(y_Q - y_{\bar{Q}})})$$

The propagator therefore always remains off-shell, since $m_T^2 \geq m_Q^2$. This is in fact true for all propagators that appear in diagrams for heavy quark production. The addition of the mass scale m_T sets a lower bound for the propagators. It would not occur if we consider the production of light quarks, where the appropriate cut-off would be the scale Λ_{QCD}. In contrast, as long as the quark is sufficiently heavy ($m_Q >> \Lambda_{QCD}$), the mass sets a scale at which perturbation theory is expected to hold.

4.5 Higgs boson(s)

The experimental observation of one or more Higgs bosons will be fundamental for accepting the Standard model. In the Standard model, one doublet of scalar fields is assumed, thus leading to the existence of one neutral scalar particle H. The Higgs boson mass is not theoretically predictable. We can only bound this

mass to upper and lower bound to the range $130 < m_H < 190$ GeV[6]. If we take cutoff 1 TeV, the range widens to $50 < m_H < 800$ GeV[6]. In supersymmetric models, the Higgs sector contains at least two doublets of scalar fields. The MSSM model predicts 5 physical Higgs particles: CP-even ones h,H;CP-odd one A;charged ones $H^{\pm}$. The lightest one is supposed to have mass up to 150 GeV. Further extension can be SUSY as the maximal possible extension of the Lorentz group.
The largest rate for Higgs boson production at LHC will come from the gluon fusion process

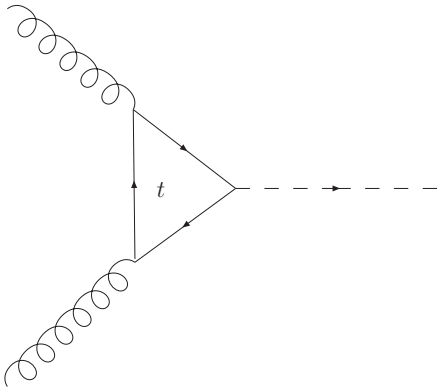

Figure 4.5: Feynman diagrams for Higgs boson production

Higgs boson couples to fermions with a strength proportional to the fermion mass. Therefore, the largest contribution results from the top quark. But in general any quark is allowed to circulate in the loop. Since the LO diagram already contains a loop, the production of a Higgs boson is considerably harder to calculate. Thus it is convenient to formulate the diagram as an effective coupling of the Higgs boson to two gluons in the limit that the top quark is infinitely massive. Surprisingly it is not necessary to have all other scales in the problem much smaller than m_T if we want to use such approximation. In fact, only $m_H < m_T$ is needed[2] (and $p_T(jets) < m_T$ if there are any jets present). With this approximation the NNLO has been calculated so far. The second largest Higgs boson cross-section at LHC results from the weak boson fusion mechanism, which proceeds via the exchange of W and Z boson from incoming quarks

Although this procedure is an electroweak one and so proceeds at a slower rate, it has a very clear experimental signature. The incoming quarks only receive a small kick through the radiation of W/Z bosons, so they can be detected as jets very forward and backward at large absolute rapidities. Furthermore, very little hadronic radiation is expected in the central region of the detector since no coloured particles are exchanged between quarks. Therefore, some kind of "rapidity gap" will be present in the hadronic calorimeters.

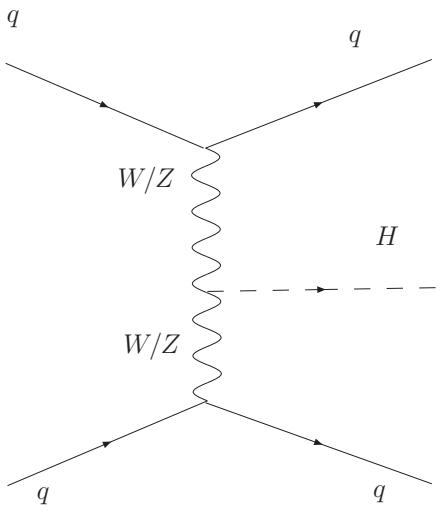

Figure 4.6: Feynman diagrams for Higgs boson production

4.6 Beyond Standard model

There is a variety of possible physics in extensions of the Standard model. Technicolor models replace Higgs bosons with dynamical condensates. This will lead to flavour changing neutral currents and violations of precision elecroweak data. Although there is no standard technicolor model, the basic idea could solve the hierarchy problem at a scale about 1 TeV. Other phenomena, which are not predicted by any specific model, such as excited quarks, leptoquarks, contact interactions can lead directly to new physics[6]. New gauge bosons are predicted by the extension of the electroweak gauge group. Finally, monopoles might explain the quantization of charge.

Chapter 5

Results of analysis

5.1 Files, analysis tools

The main goal of this work is to analyze the asymmetry of electron-positron production in the Drell-Yan process. There are two sets of data used for the analysis. Both were generated by Pythia in version 6.221 [7]. Steering parameters used for getting the appropriate process are included in the Appendix. Schematically

$$pp \rightarrow X + Z \rightarrow e^+e^- \quad \text{at 14 TeV}$$

The first set contained 1000000 interactions $Z \rightarrow ee$. The matrix element was composed only from the Z boson intermediate propagator

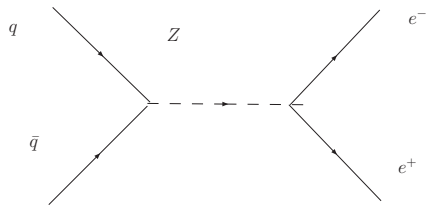

Figure 5.1: Drell-Yan process via Z boson only

The resulting cross section is $(1,554 \pm 0,0084) * 10^6 fb$.
The second set contained 5000000 interactions $Z \rightarrow ee$. The matrix element was composed from Z boson and γ intermediate propagator.

The resulting cross section is $1,580 * 10^6 fb$. The analysis has been performed using ROOT in production version 5.14[8].

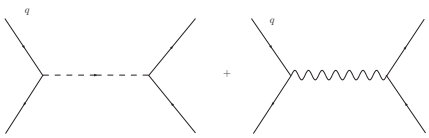

Figure 5.2: Drell-Yan process via Z boson and gamma

5.2 Event selection, analyzed objects

For the purpose of analysis certain objects were used (on the generator level). It was mainly the generated Z boson, e^+e^- leptons, the secondary reconstructed Z boson and e^+e^- lepton pair(see Chapter 2.2). Let's note that the data set was generated to have the Z boson in the inter-medial state and electrons and positrons in the final state. But here, we are using the only situation, where exactly one electron and one positron is created. Therefore, by the means of "all events" this selection has to be understand. The difference has the value of approximately 3%. Also some of Z boson kinematical characteristics were analyzed. The selection lead to the following event classes

- $P_t > 20GeV$ for e^+e^- pair
  1. both e^+e^- has $|\eta| < 2,5$
  2. one of e^+e^- has $|\eta| \in < 2,5; 3,2 >$ and the other $|\eta| < 2,5$
  3. both e^+e^- has $|\eta| \in < 2,5; 3,2 >$
- $P_t > 20GeV$ for e^+e^- pair
  1. both e^+e^- has $|\eta| < 2,5$
  2. one of e^+e^- has $|\eta| \in < 2,5; 5,0 >$ and the other $|\eta| < 2,5$
  3. both e^+e^- has $|\eta| \in < 2,5; 5,0 >$
- $P_t > 20GeV$ for e^+e^- pair
  1. both e^+e^- has $|\eta| < 2,5$
  2. one of e^+e^- has $|\eta| \in < 2,5; 7,5 >$ and the other $|\eta| < 2,5$
  3. both e^+e^- has $|\eta| \in < 2,5; 7,5 >$

5.3 Dependence of forward-backward asymmetry and kinematics distributions on the cuts applied on the secondary electrons

Now, some results will be presented. For each kinematical cut the appropriate cross section is presented. It is counted according to the formula

$$\sigma_i = \frac{N_i}{N}\sigma_{tot}$$

where N_i is the number of events in this cut, N is the total number of events and σ_{tot} is the total cross section. The second value for each process will be the cross section with the reconstruction and identification efficiency taken into account of the value 70%[5].

Tab.1:First set

Event class	σ $[*10^6 fb]$	σ with eff. 70% $[*10^6 fb]$	Number of events
all events	1,520	0.745	978157
$\|\eta\| < 2,5$ both	0.746	0.366	479773
$\|\eta\| \in < 2,5;3,2 >$ one	0.212	0.104	136435
$\|\eta\| \in < 2,5;3,2 >$ both	0.052	0.025	33511
$\|\eta\| \in < 2,5;5,0 >$ one	0.282	0.138	181245
$\|\eta\| \in < 2,5;5,0 >$ both	0.112	0.055	71909
$\|\eta\| \in < 2,5;7,5 >$ one	0.287	0.141	184640
$\|\eta\| \in < 2,5;7,5 >$ both	0.121	0.059	77638

Tab.2:Second set

Event class	σ $[*10^6 fb]$	σ with eff. 70% $[*10^6 fb]$	Number of events
all events	1.546	0.758	4891420
$\|\eta\| < 2,5$ both	0.759	0.372	2401558
$\|\eta\| \in < 2,5;3,2 >$ one	0.216	0.106	682004
$\|\eta\| \in < 2,5;3,2 >$ both	0.053	0.026	168808
$\|\eta\| \in < 2,5;5,0 >$ one	0.286	0.140	906453
$\|\eta\| \in < 2,5;5,0 >$ both	0.114	0.056	360198
$\|\eta\| \in < 2,5;7,5 >$ one	0.292	0.143	923987
$\|\eta\| \in < 2,5;7,5 >$ both	0.123	0.060	389045

The next part of the analysis results will contain forward-backward asymmetry values for both sets and each kinematical cut.

Tab.3:Asymetry for the first set

Event class	A_{FB} $[*10^{-2}]$	Statistical error $[*10^{-2}]$
all events	3.834	0.1429
$\|\eta\| < 2,5$ both	2.495	0.2042
$\|\eta\| \in < 2,5;3,2 >$ one	4.662	0.3829
$\|\eta\| \in < 2,5;3,2 >$ both	6.496	0.7725
$\|\eta\| \in < 2,5;5,0 >$ one	5.571	0.3322
$\|\eta\| \in < 2,5;5,0 >$ both	6.446	0.5274
$\|\eta\| \in < 2,5;7,5 >$ one	5.607	0.3291
$\|\eta\| \in < 2,5;7,5 >$ both	6.772	0.5076

Tab.4:Asymetry for the second set

Event class	A_{FB} $[*10^{-2}]$	Statistical error$[*10^{-2}]$
all events	4.189	0.0639
$\|\eta\| < 2,5$ both	2.852	0.0913
$\|\eta\| \in < 2,5;3,2 >$ one	5.884	0.1712
$\|\eta\| \in < 2,5;3,2 >$ both	6.557	0.3442
$\|\eta\| \in < 2,5;5,0 >$ one	6.960	0.1485
$\|\eta\| \in < 2,5;5,0 >$ both	6.625	0.2356
$\|\eta\| \in < 2,5;7,5 >$ one	7.084	0.1471
$\|\eta\| \in < 2,5;7,5 >$ both	6.702	0.2267

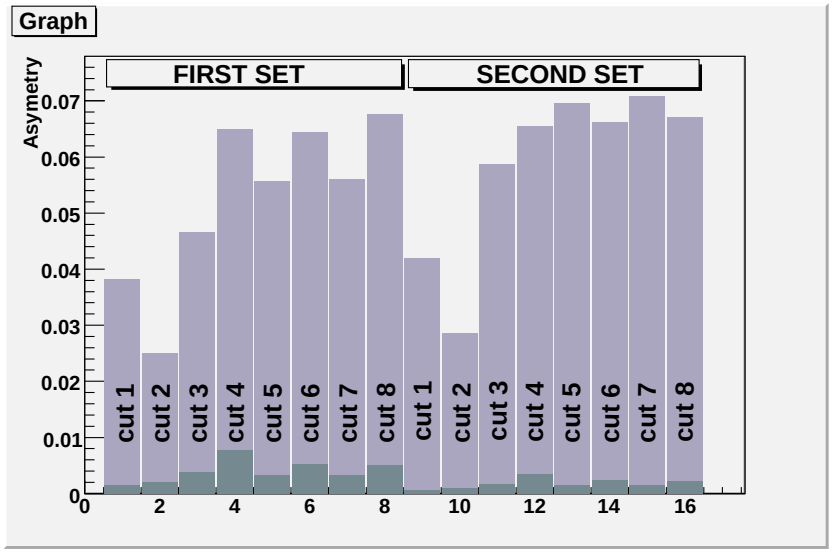

Figure 5.3: Asymetry bar chart

We will also present some kinematical variables distributions for the Z boson. Namely the invariant mass in the region 0-200GeV, the rapidity in the region (-10,10) and the p_T in the region 0-100GeV will be shown. The first three histograms correspond to the first set of data and the second three histograms correspond to the second set.

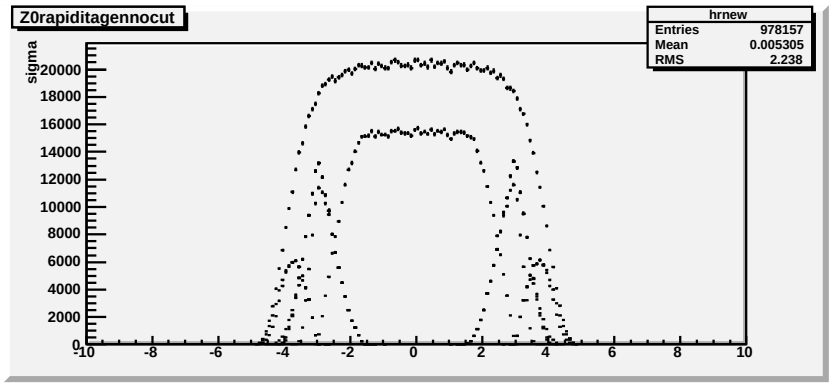

Figure 5.4: The rapidity distribution for generated Z boson from the first set

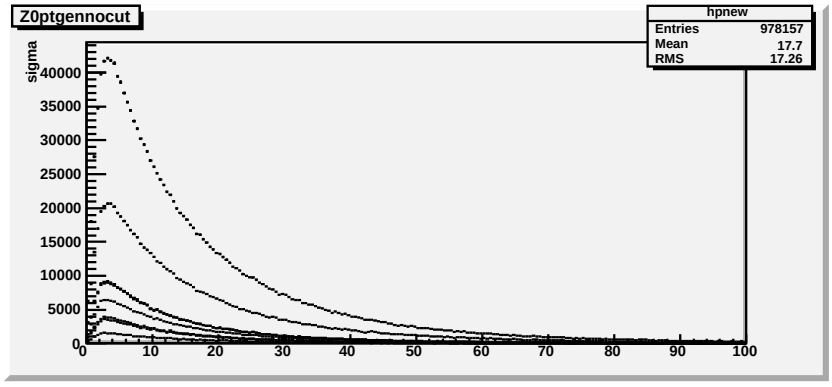

Figure 5.5: The p_T distribution for generated Z boson from the first set

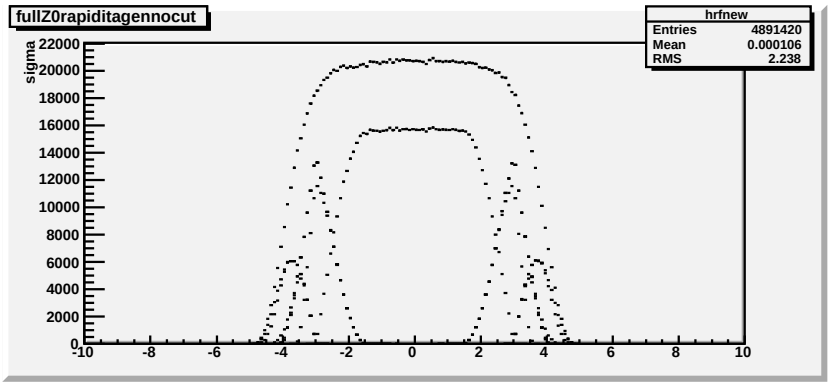

Figure 5.6: The rapidity distribution for generated Z boson from the second set

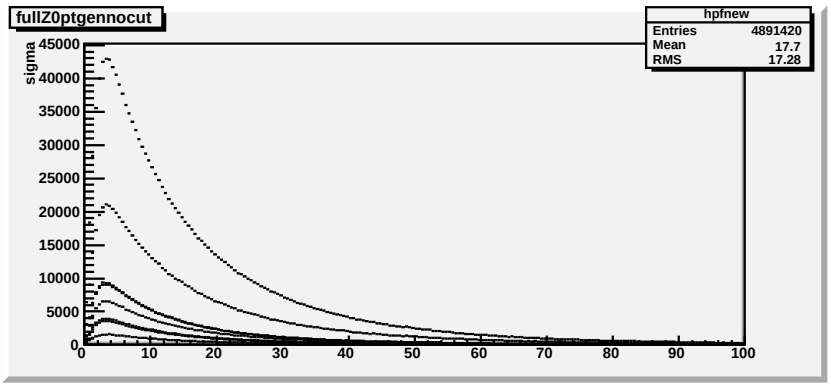

Figure 5.7: The p_T distribution for generated Z boson from the second set

For the analysis of the invariant mass, three formulas were used for the fitting. It is Gauss formula, Breit-Wigner formula and a relativistic variant of Breit-Wigner. Gaussian parameter σ is converted to the corresponding FWHM Γ for the purpose of the comparison.

Gauss formula $$\sigma_{\mathrm{GA}} \sim \frac{1}{\sqrt{2\pi}\sigma} e^{-\frac{(m-M_Z)^2}{2\sigma^2}}$$

Breit – Wigner formula $$\sigma_{\mathrm{BW}} \sim \frac{\Gamma_0^2}{(m-M_Z)^2 + (\frac{\Gamma_0}{2})^2}$$

Relativistic Breit – Wigner formula $$\sigma_{\mathrm{RBW}} \sim \frac{m^2 \frac{\Gamma_0^2}{M_Z^2}}{(m^2 - M_Z^2)^2 + m^4 \frac{\Gamma_0^2}{M_Z^2}}$$

$$\Gamma_0 = 2\sqrt{2ln2}\sigma$$

Γ_0 average Z width

M_Z average Z mass

Figure 5.8: Fitting functions for invariant mass distribution

Statistical parameters for each fit were studied and they are summarized in following graphs.

Here is the mean of mass distribution fits. The yellow bar indicates currently accepted value of the Z boson mass. The relativistic Breit-Wigner gives the

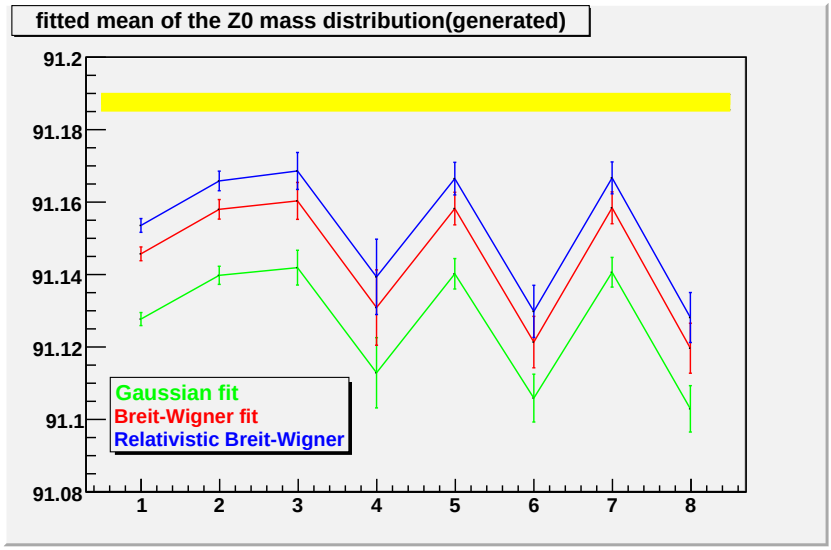

Figure 5.9: fitted mean for Z boson mass distributions for generated Z boson

best approximation for generated data while the Gaussian distribution gives the worst. All mean values are below the PDG Z boson mass.

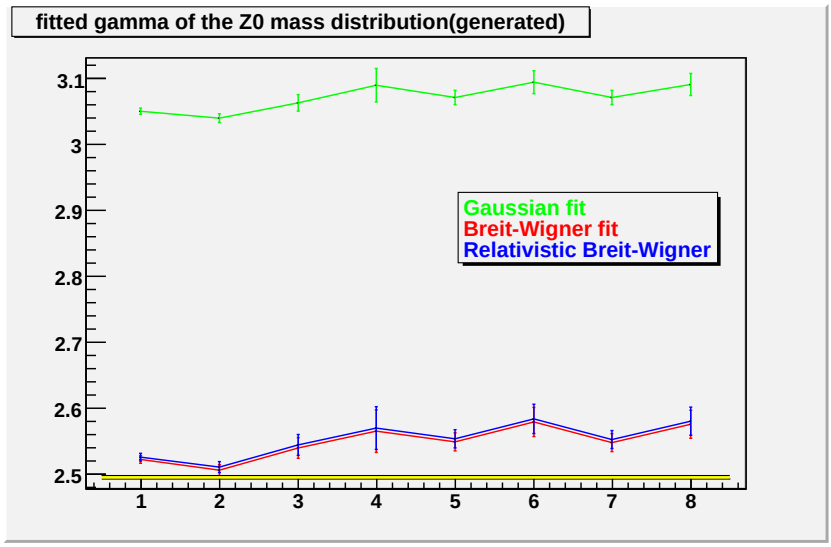

Figure 5.10: fitted gamma for Z boson mass distributions for generated Z boson

In the case of Γ, the gaussian fit gives the worst results too. Both Breit-

Wigner and a relativistic variant gives almost the same results.

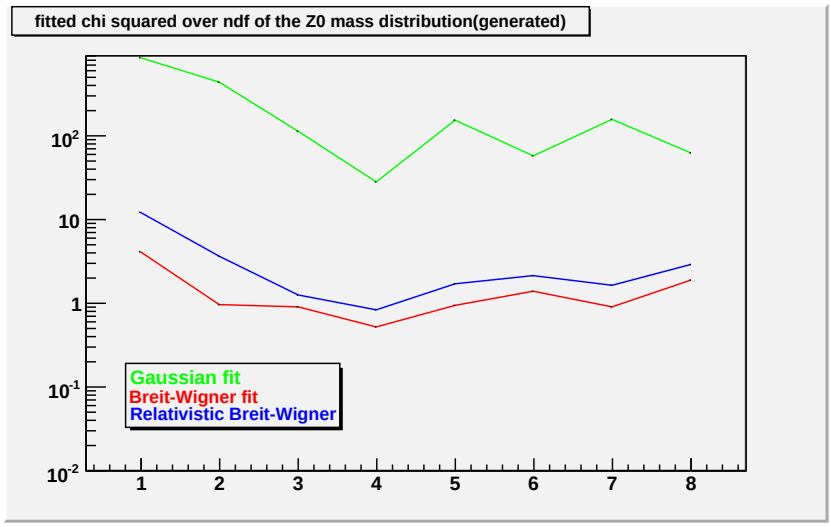

Figure 5.11: fitted χ^2/ndf for Z boson mass distributions for generated Z boson

For the χ^2 over the number of degrees of freedom, results are best for the Breit-Wigner distribution. Although a relativistic Breit-Wigner gives more accurate prediction for M_Z and Γ than the non-relativistic variant, it is not the best fit. It is obvious that gaussian fit do not describe the distribution well.

In the case of the secondary Z boson reconstructed from electron positron pair, the mean of all fits have greater deviation from predicted Z boson mass than for the generated Z boson. Still the best fit is the relativistic Breit-Wigner formula.

The Γ fit shows that Gaussian fit is the worst of all. The deviation between non-relativistic and relativistic formula is negligible here.

The χ^2 over number of degrees of freedom graph shows the same order of tested distributions as for the generated Z boson case. The gaussian fit has the worst agreement with data, while Breit-Wigner agrees most. Here, the difference between both variants of Breit-Wigner is smaller than for the generated Z boson. But there is one important difference with respect to the generated case - no one distribution is consistent with data.

Next variable used for the analysis is the p_T distribution. The graph of means for each cut is presented.

As errors, the RMS divided by the square root of the number of events in each cut was used. The mean for secondary Z boson is shifted slightly to higher values than the generated Z boson means.

This graph summarizes the rapidity distributions for each cut in the case of generated Z boson. Here we can see how that cuts were chosen. The most important cut is the second one.

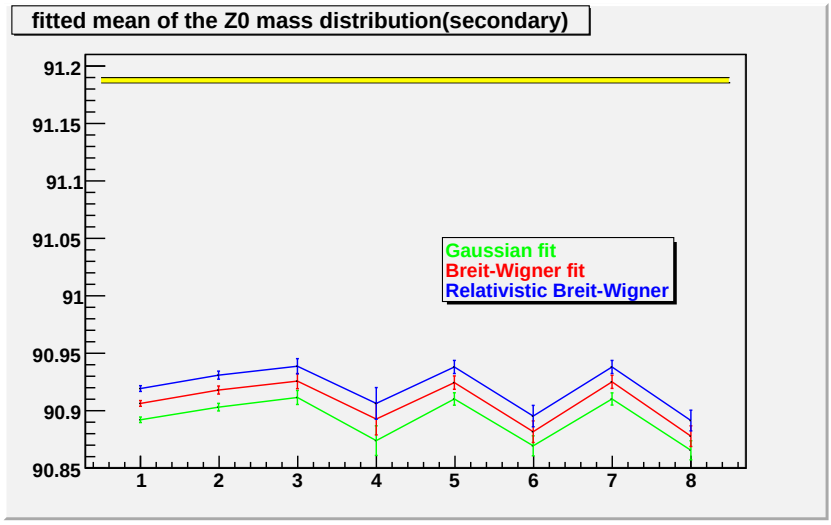

Figure 5.12: fitted mean for Z boson mass distributions for secondary Z boson

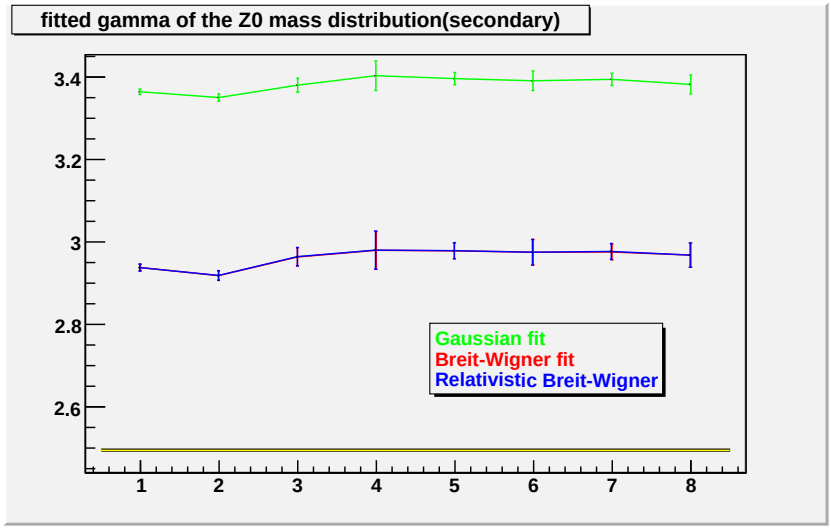

Figure 5.13: fitted gamma for Z mass distributions for secondary Z boson

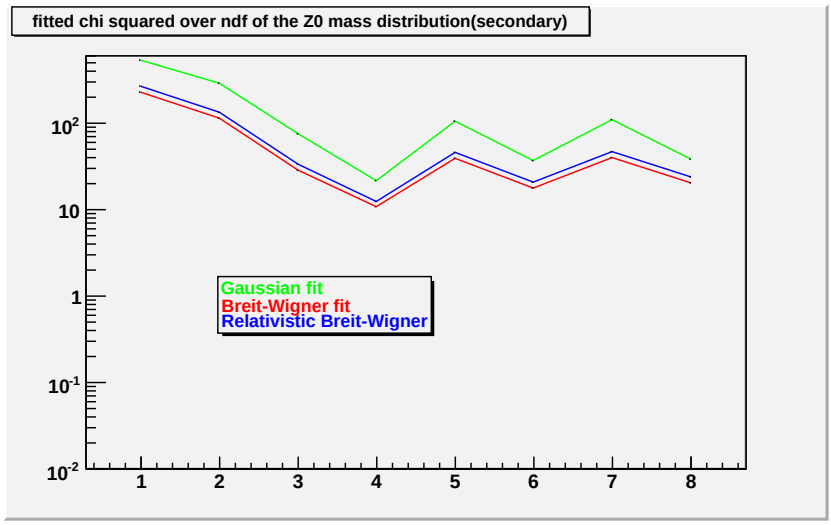

Figure 5.14: fitted χ^2/ndf for Z mass distributions for secondary Z boson

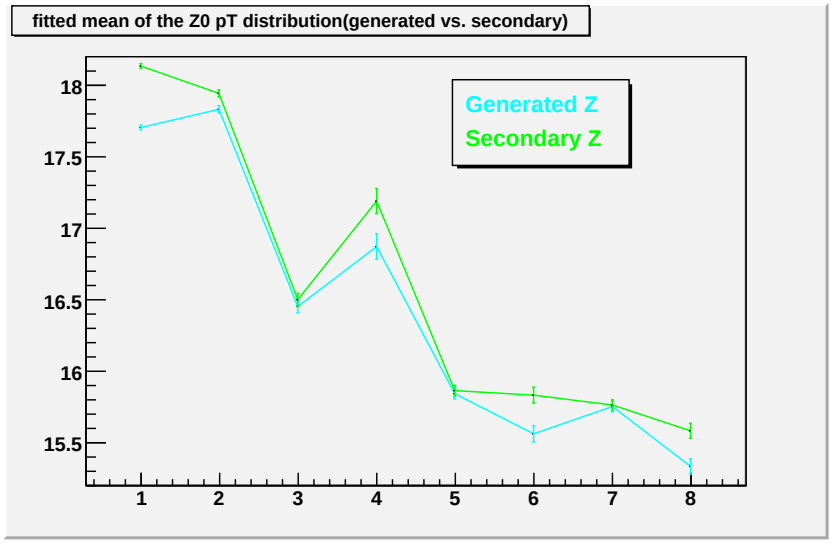

Figure 5.15: fitted mean for Z boson p_T distributions

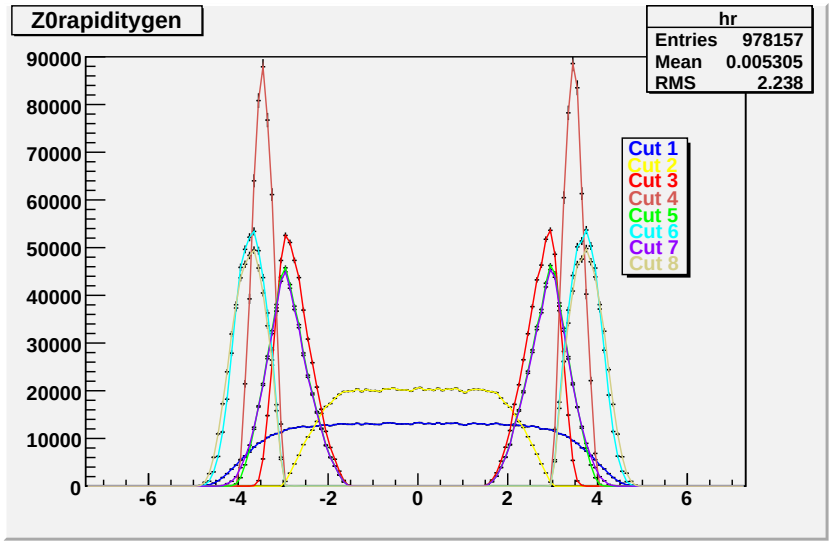

Figure 5.16: Rapidity distributions for each cut

Chapter 6

Conclusions

The asymmetry for each cut is presented with corresponding statistical errors. Second cut shows most symmetric configuration, while the last cut is most asymmetric. The Dependence of multiplicities and cross-sections on kinematic cuts applied on the Z boson secondaries is also presented. 48% of Z to ee contained in the standard ATLAS acceptance window for electrons ($p_T > 20GeV$ and $|\eta| < 2,5$) Distributions of the invariant mass of generated Z boson is best described by both Breit-Wigner distributions for all investigated classes of events. Parameters of relativistic Breit-Wigner are most similar to the PDG values. For secondary Z boson no one of tested distributions is consistent with data. Furthermore, differences between PDG values and data fits are greater than for generated Z boson.

Appendices

Steering parameters of generated events for Pythia

Pythia.PythiaCommand = {

"pysubs msel 0",
"pysubs msub 1 1",
"pypars mstp 43 2",
"pysubs ckin 1 81.",
"pydat3 mdme 174 1 0",
"pydat3 mdme 175 1 0",
"pydat3 mdme 176 1 0",
"pydat3 mdme 177 1 0",
"pydat3 mdme 178 1 0",
"pydat3 mdme 179 1 0",
"pydat3 mdme 182 1 1",
"pydat3 mdme 183 1 0",
"pydat3 mdme 184 1 0",
"pydat3 mdme 185 1 0",
"pydat3 mdme 186 1 0",
"pydat3 mdme 187 1 0",
"pypars mstp 82 4",
"pydat1 mstj 22 2",
"pydat1 mstj 11 3",
"pydat1 parj 54 -0.07",
"pydat1 parj 55 -0.006",
"pypars parp 82 1.8",
"pypars parp 84 0.5",
"pydat3 mdcy 15 1 0",
"pyinit pylisti 12",
"pyinit pylistf 1",
"pystat 1 3 4 5",
"pyinit dumpr 1 5",
"pypars mstp 128 0"};

End of job options file

Chapter 7

References

[1] Francis Halzen & Alan D. Martin, Quarks and leptons:An introductory course in modern particle physics, John Wiley & Sons Inc. New York,USA, 1984, pages 33-67

[2] J.M.Campbell, J.W.Huston and W.J.Stirling, Hard interactions of quarks and gluons: a primer for LHC physics, Rep. Prog. Phys. 70(2007) 89-193

[3] B. Webber, Ann. Rev. Nucl. Part. Sci., 36, 253-286(1986)

[4] J. Horejsi, Fundamentals of electroweak theory, Charles university in Prague, Czech Republic, 2002

[5] ATLAS Detector and physics performance, Technical Dasign Report,Volume I, CERN/LHC/99-14,1999

[6] ATLAS Detector and physics performance, Technical Dasign Report,Volume II, CERN/LHC/99-15,1999

[7] T. Sjoestrand, P.Eden, C.Friberg, L.Loennblad, G.Miu, S. Mrenna and E.Norrbin, Pythia 6.2, Computer Physics Commun. 135, 238(2001)

[8] ROOT: http://root.cern.ch

[9] George Sterman et al., Handbook of perturbative QCD, Rev. Mod. Phys.,67, 1, 157-248(1986)

[10] http://indico.cern.ch/conferenceDisplay.py?confId=12055

7.1 Bibliography

[1] W.Greiner, B.Muller, Quantum chromodynamics, Springer Berlin 2000

[2] Josef Zacek, Uvod do fyziky elementarnich castic, Carolinum publishing Prague, Czech Republic, 2005

[3] John C. Collins and David E. Soper, Angular distribution of dileptons in high-energy collisions, Phys.Rev. D 16, 7, 2219-2225(1977)